

Soft-photon radiation in high-energy proton-proton collisions within the tensor-Pomeron approach: Bremsstrahlung

Piotr Lebiedowicz^{1,*}, Otto Nachtmann^{2,†} and Antoni Szczurek^{1,‡,§}

¹*Institute of Nuclear Physics Polish Academy of Sciences, Radzikowskiego 152, PL-31342 Kraków, Poland*

²*Institut für Theoretische Physik, Universität Heidelberg, Philosophenweg 16, D-69120 Heidelberg, Germany*



(Received 17 June 2022; accepted 12 July 2022; published 23 August 2022)

We discuss diffractive processes in proton-proton collisions at small momentum transfers without and with photon radiation. We consider the soft exclusive reactions $pp \rightarrow pp$, $p\bar{p} \rightarrow p\bar{p}$, and $pp \rightarrow pp\gamma$ within the tensor-Pomeron and vector-odderon approach. We compare our results with the data for pp and $p\bar{p}$ total cross sections, for the ratio of real to imaginary parts of the forward scattering amplitude, and for the elastic pp cross sections, especially those from TOTEM. To describe the low-energy data more accurately, the secondary reggeons must be included. We write down the amplitudes for the photon bremsstrahlung in high-energy proton-proton collisions using the tensor-Pomeron model. These results are relevant for the c.m. energies presently available at the Relativistic Heavy Ion Collider and at the LHC. We present predictions for the proposed measurements of soft photons with the planned future upgrade of the ALICE experiment at the LHC. We investigate the limits of applicability of the soft-photon approximation (SPA) based on Low's theorem. The corresponding SPA results are compared to those obtained from our complete model. The regions of phase space are given quantitatively where SPA and our complete tensor-Pomeron results are close to each other. As an example, let k_{\perp} , y , and ω , be the absolute value of the transverse momentum, the rapidity, and the energy of the photon, respectively, in the overall c.m. system. For the region $1 \text{ MeV} < k_{\perp} < 100 \text{ MeV}$ and $3.5 < |y| < 5.0$, we find that the SPA Ansatz with only the pole terms $\propto \omega^{-1}$ agrees at the percent level with our complete model result up to $\omega \cong 2 \text{ GeV}$.

DOI: [10.1103/PhysRevD.106.034023](https://doi.org/10.1103/PhysRevD.106.034023)

I. INTRODUCTION

With this article, we continue our investigations of soft-photon radiation in diffractive hadronic high-energy reactions. In Ref. [1], we treat, as a first example using our approach, high-energy $\pi\pi$ scattering without and with photon radiation. In the present paper, we extend these considerations to pp and $p\bar{p}$ scattering.

The emission of soft photons, that is, photons of energy ω approaching zero, was treated in the seminal paper by Low [2]. In that paper, it was shown that the term of order ω^{-1} in the amplitude for the emission reaction can

be obtained from the amplitude without photon emission. To this order, the emission comes exclusively from the external particles, and this is a strict consequence of Quantum Field Theory (QFT). Many soft-photon approximations (SPAs) are based on this result.

Experimental studies trying to verify Low's theorem [3–14] have, in many cases, found large deviations from the SPA calculations. For a review of the experimental and theoretical situations, see Ref. [15]. Clearly, more experimental and theoretical work is needed in order to clarify this so-called soft-photon problem.

From the experimental side, there is, for instance, the plan for a new multipurpose detector at the LHC, ALICE 3 [16]. One physics aim for this new initiative is a measurement of ultrasoft photons at very low transverse momentum in pp , pA , and AA collisions; see, e.g., Refs. [17,18].

From the theoretical side, many authors have studied soft-photon production following Ref. [2]; see, for instance, Refs. [19–27]. In our paper [1], we have presented two types of soft-photon studies.

- (1) We have studied the amplitude for the reaction $\pi\pi \rightarrow \pi\pi\gamma$ in the limit of the photon c.m. energy ω going to zero. Using only rigorous QFT methods, we have calculated the terms of order ω^{-1} and ω^0 . We found

*Piotr.Lebiedowicz@ifj.edu.pl

†O.Nachtmann@thphys.uni-heidelberg.de

‡Antoni.Szczurek@ifj.edu.pl

§Also at College of Natural Sciences, Institute of Physics, University of Rzeszów, ul. Pigońia 1, PL-35310 Rzeszów, Poland.

Published by the American Physical Society under the terms of the Creative Commons Attribution 4.0 International license. Further distribution of this work must maintain attribution to the author(s) and the published article's title, journal citation, and DOI. Funded by SCOAP³.

agreement with the result of Low [2] for the ω^{-1} term but, we disagreed with the ω^0 term of Ref. [2]. We have analyzed the origin of this disagreement, and we give a critique of the corresponding results of the papers [2,20,22–26] in Appendixes A and B of Ref. [1].

- (2) We have discussed the reactions $\pi\pi \rightarrow \pi\pi$ and $\pi\pi \rightarrow \pi\pi\gamma$ at high energies in a specific model, the tensor-Pomeron model of Ref. [28]. The “standard” results obtained in this approach were then compared to various soft-photon approximations.

With the present paper, we continue our line (2) of research. Further results from the line (1) will be presented elsewhere.

One class of hadronic reactions one can study at the LHC is exclusive diffractive proton-proton collisions. Examples are $pp \rightarrow pp$ elastic scattering and central exclusive production of mesons, for instance, $pp \rightarrow pp\pi^+\pi^-$. In this paper, we present the results of our investigations of the following soft reactions at small momentum transfer:

$$\begin{aligned} p + p &\rightarrow p + p, \\ p + \bar{p} &\rightarrow p + \bar{p}, \\ p + p &\rightarrow p + p + \gamma. \end{aligned} \quad (1.1)$$

We shall work within the tensor-Pomeron model as proposed in Ref. [28] for soft hadronic high-energy reactions. There, the soft Pomeron and the charge conjugation $C = +1$ reggeons are described as effective rank-2 symmetric tensor exchanges, and the odderon and the $C = -1$ reggeons are described as effective vector exchanges. Now, our task is to construct a soft-photon diffractive amplitude of the $pp \rightarrow pp\gamma$ reaction which satisfies all theoretical constraints.

Before coming to our present investigations, we make remarks on some related works. Exclusive diffractive photon bremsstrahlung in pp collisions was discussed earlier in Refs. [29–31] within other approaches. The bremsstrahlung-type emission of ω and π^0 mesons was calculated in Refs. [32,33]. It is also worth noting that the $pp \rightarrow pp\gamma$ reaction has not yet been measured at high energies; however, feasibility studies were performed for RHIC energies [34] and for LHC energies [35,36].

The theoretical methods which we shall develop in the present paper for soft-photon production can also be used in a completely different context: for the production of “dark photons”. Indeed, an interesting proposal of new physics search was discussed recently in Ref. [37]: to study the forward production of dark vectors (photons) and scalars via bremsstrahlung in proton-proton collisions with the proposed Forward Physics Facility (FPF) at the High-Luminosity LHC [38]. At the LHC, such weakly coupled long-lived particles, with masses $m \sim 10 \text{ MeV} - 1 \text{ GeV}$, could be produced through light meson decays and

bremsstrahlung in the region that would be covered by the FPF.

Our present paper is organized as follows. In Sec. II, we discuss the amplitudes for the reactions listed in (1.1) within the tensor-Pomeron approach. In Sec. III, we describe two SPAs based on Low’s theorem. The results of our calculations are presented in Sec. IV. Section IV A is devoted to a comparison of the model results to the available data on the total and elastic pp and $p\bar{p}$ cross sections. In Sec. IV B, we present our “exact” model or “standard” results for the $pp \rightarrow pp\gamma$ reaction and a comparison to SPAs. Section IV C contains comments on the photon radiation in connection with diffractive excitation of the proton. Section V contains a summary and our conclusions. Some details of the present model are given in Appendixes A and B.

Throughout our paper, we use the metric and γ -matrix conventions of Ref. [39].

II. REACTIONS $pp \rightarrow pp$, $p\bar{p} \rightarrow p\bar{p}$, AND $pp \rightarrow pp\gamma$

Here, we discuss the reactions

$$p(p_a, \lambda_a) + p(p_b, \lambda_b) \rightarrow p(p_1, \lambda_1) + p(p_2, \lambda_2), \quad (2.1)$$

$$p(p_a, \lambda_a) + \bar{p}(p_b, \lambda_b) \rightarrow p(p_1, \lambda_1) + \bar{p}(p_2, \lambda_2), \quad (2.2)$$

and

$$p(p_a, \lambda_a) + p(p_b, \lambda_b) \rightarrow p(p'_1, \lambda_1) + p(p'_2, \lambda_2) + \gamma(k, \epsilon). \quad (2.3)$$

The momenta are denoted by p_a, \dots, k ; the helicities of the protons are denoted by $\lambda_a, \dots, \lambda_2$; and ϵ is the polarization vector of the photon. The energy-momentum conservation in (2.1), (2.2), and (2.3) requires

$$p_a + p_b = p_1 + p_2, \quad (2.4)$$

$$p_a + p_b = p'_1 + p'_2 + k. \quad (2.5)$$

We consider soft hadronic high-energy reactions. We use standard formulas of the tensor-Pomeron and vector-odderon model from Ref. [28]. In this model, the assumption is made that the Pomeron \mathbb{P} and the charge-conjugation $C = +1$ reggeons $f_{2\mathbb{R}}$, $a_{2\mathbb{R}}$ couple to hadrons like symmetric tensors of rank 2, and the odderon \mathbb{O} and the $C = -1$ reggeons $\omega_{\mathbb{R}}$, $\rho_{\mathbb{R}}$ couple to hadrons like vectors. We do not treat γ exchange in the following.

In Ref. [40], it is shown that the experimental results [41] on the spin dependence of high-energy proton-proton elastic scattering exclude a scalar character of the Pomeron couplings but are perfectly compatible with the tensor-Pomeron model. A vector coupling for the Pomeron could definitely be ruled out as shown in Ref. [42].

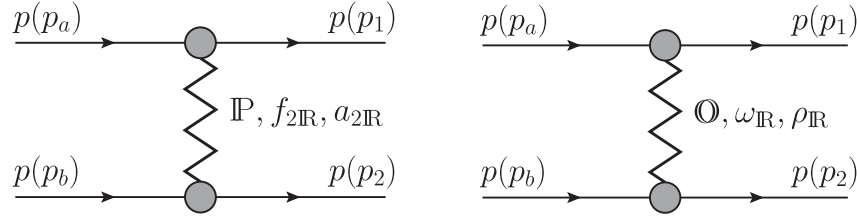


FIG. 1. The diagrams for $pp \rightarrow pp$ elastic scattering with $C = +1$ (left) and $C = -1$ (right) exchanges. There are also the diagrams corresponding to the exchange $p_1 \leftrightarrow p_2$.

A. Reaction $pp \rightarrow pp$

We consider first the reaction (2.1) for off-shell protons. Also, here, energy-momentum conservation (2.4) holds. We have the diagrams of Fig. 1 with $C = +1$ and $C = -1$ exchanges. The kinematic variables are

$$\begin{aligned} s &= (p_a + p_b)^2 = (p_1 + p_2)^2, \\ t &= (p_a - p_1)^2 = (p_b - p_2)^2, \\ u &= (p_a - p_2)^2 = (p_b - p_1)^2, \\ m_a^2 &= p_a^2, \quad m_b^2 = p_b^2, \quad m_1^2 = p_1^2, \quad m_2^2 = p_2^2. \end{aligned} \quad (2.6)$$

The interchange $p_1 \leftrightarrow p_2$ implies $t \leftrightarrow u$, where $u = -s - t + m_a^2 + m_b^2 + m_1^2 + m_2^2$. We are interested in the kinematic region

$$\sqrt{s} \gg m_p, \quad \sqrt{|t|} \lesssim m_p, \quad s \gg |m_a^2|, |m_b^2|, |m_1^2|, |m_2^2|. \quad (2.7)$$

There, we can neglect the diagrams with $p_1 \leftrightarrow p_2$.

We denote the off-shell pp scattering amplitude by

$$\mathcal{M}^{(0)}(p_a, p_b, p_1, p_2). \quad (2.8)$$

In the tensor-Pomeron model [28], all exchanges at high energies are assumed to be describable by effective single Regge poles. Some standard references to Regge theory are Refs. [43–45]. For further literature, we refer to Refs. [1,28]. The special feature of the tensor-Pomeron model is, as mentioned above, that all $C = +1$ exchanges (\mathbb{P} , $f_{2\mathbb{R}}$, $a_{2\mathbb{R}}$) are described as effective rank-2 symmetric tensor exchanges and that all $C = -1$ exchanges (\mathbb{O} , $\omega_{\mathbb{R}}$, $\rho_{\mathbb{R}}$) are described as effective vector exchanges. To calculate the expressions for the diagrams of Fig. 1, we need the effective propagators for the exchange objects and their proton-proton coupling vertices. All these quantities are listed in Chap. 3 of Ref. [28].

To write down the amplitude (2.8) in this model in a convenient way, we define for the $C = +1$ exchanges the functions

$$\mathcal{F}_{\mathbb{P}pp}(s, t) = [3\beta_{\mathbb{P}pp} F_1(t)]^2 \frac{1}{4s} (-is\alpha'_{\mathbb{P}})^{\alpha_{\mathbb{P}}(t)-1}, \quad (2.9)$$

$$\mathcal{F}_{f_{2\mathbb{R}}pp}(s, t) = \left[\frac{g_{f_{2\mathbb{R}}pp}}{M_0} F_1(t) \right]^2 \frac{1}{4s} (-is\alpha'_{f_{2\mathbb{R}}})^{\alpha_{f_{2\mathbb{R}}}(t)-1}, \quad (2.10)$$

$$\mathcal{F}_{a_{2\mathbb{R}}pp}(s, t) = \left[\frac{g_{a_{2\mathbb{R}}pp}}{M_0} F_1(t) \right]^2 \frac{1}{4s} (-is\alpha'_{a_{2\mathbb{R}}})^{\alpha_{a_{2\mathbb{R}}}(t)-1} \quad (2.11)$$

and for the $C = -1$ exchanges the functions

$$\mathcal{F}_{\mathbb{O}pp}(s, t) = -\eta_{\mathbb{O}} [3\beta_{\mathbb{O}pp} F_1(t)]^2 (-is\alpha'_{\mathbb{O}})^{\alpha_{\mathbb{O}}(t)-1}, \quad (2.12)$$

$$\mathcal{F}_{\omega_{\mathbb{R}}pp}(s, t) = \left[\frac{g_{\omega_{\mathbb{R}}pp}}{M_-} F_1(t) \right]^2 (-is\alpha'_{\omega_{\mathbb{R}}})^{\alpha_{\omega_{\mathbb{R}}}(t)-1}, \quad (2.13)$$

$$\mathcal{F}_{\rho_{\mathbb{R}}pp}(s, t) = \left[\frac{g_{\rho_{\mathbb{R}}pp}}{M_-} F_1(t) \right]^2 (-is\alpha'_{\rho_{\mathbb{R}}})^{\alpha_{\rho_{\mathbb{R}}}(t)-1}. \quad (2.14)$$

We define also the following quantities:

$$\mathcal{F}_T(s, t) = \mathcal{F}_{\mathbb{P}pp}(s, t) + \mathcal{F}_{f_{2\mathbb{R}}pp}(s, t) + \mathcal{F}_{a_{2\mathbb{R}}pp}(s, t), \quad (2.15)$$

$$\mathcal{F}_V(s, t) = \mathcal{F}_{\mathbb{O}pp}(s, t) + \mathcal{F}_{\omega_{\mathbb{R}}pp}(s, t) + \mathcal{F}_{\rho_{\mathbb{R}}pp}(s, t). \quad (2.16)$$

All quantities occurring in (2.9)–(2.14) are as defined in Chaps. 3.1 and 3.2 of Ref. [28]. To make our article self-contained, we give in Appendix A a list of the quantities and their values which we use. In considering the effective propagators and vertices, some additional comments are in order:

- (i) In Ref. [28], exchange degeneracy of the reggeons with $C = +1$ ($\mathbb{R}_+ = f_{2\mathbb{R}}$, $a_{2\mathbb{R}}$) and the reggeons with $C = -1$ ($\mathbb{R}_- = \omega_{\mathbb{R}}$, $\rho_{\mathbb{R}}$) and equality of the \mathbb{R}_+ and \mathbb{R}_- trajectories was assumed; see also Ref. [46]. This leads for the trajectories to $\alpha_{\mathbb{R}}(t) = \alpha_{\mathbb{R}_+}(t) = \alpha_{\mathbb{R}_-}(t)$. We assume a standard linear form $\alpha_{\mathbb{R}}(t) = \alpha_{\mathbb{R}}(0) + \alpha'_{\mathbb{R}} t$ with the intercept and the slope: $\alpha_{\mathbb{R}}(0) = 0.5475$, $\alpha'_{\mathbb{R}} = 0.9 \text{ GeV}^{-2}$.
- (ii) The Pomeron trajectory function in (2.9) is also taken as linear in t , $\alpha_{\mathbb{P}}(t) = 1 + \epsilon_{\mathbb{P}} + \alpha'_{\mathbb{P}} t$. For the intercept parameter $\epsilon_{\mathbb{P}}$ and the slope parameter $\alpha'_{\mathbb{P}}$, we have the default values from Ref. [28]: $\epsilon_{\mathbb{P}} = 0.0808$, $\alpha'_{\mathbb{P}} = 0.25 \text{ GeV}^{-2}$. The \mathbb{P} and \mathbb{R} intercept parameters have been determined by Donnachie and Landshoff from a simultaneous fit to the pp and $p\bar{p}$ scattering data for $\sqrt{s} > 10 \text{ GeV}$ [47] and should be regarded rather as “effective” parameters. The parameter $\alpha'_{\mathbb{P}} = 0.25 \text{ GeV}^{-2}$ has been determined from the pp elastic scattering data [48] (see also Ref. [46]) and is in good agreement

with experimental findings on the exclusive ρ^0 photoproduction [49,50]. The value for the coupling constant of the Pomeron to protons is $\beta_{\mathbb{P}pp} = 1.87 \text{ GeV}^{-1}$; see (3.44) and Sec. 6.3 of Ref. [28]. For simplicity, in (2.9)–(2.14), the Dirac electromagnetic form factor of the proton is used. It is clear that this cannot be strictly correct; see the discussion in Chap. 3.2 of Ref. [46] and in Ref. [51]. It will be shown in Sec. IVA that to effectively describe the TOTEM data for the elastic pp cross section ($d\sigma/dt$) at $\sqrt{s} = 13 \text{ TeV}$, taking into account only the leading \mathbb{P} contribution, we must change in Eq. (2.9) both the $\epsilon_{\mathbb{P}}$ parameter and the Pomeron-proton form factor $F_1(t)$.

- (iii) For the odderon exchange, we will also consider an alternative Ansatz corresponding to a double Regge pole (A9). Then, we have

$$\mathcal{F}_{\mathbb{O}pp}(s, t) \rightarrow \tilde{\mathcal{F}}_{\mathbb{O}pp}(s, t) = \mathcal{F}_{\mathbb{O}pp}(s, t) \times [C_1 + C_2 \ln(-is\alpha'_0)], \quad (2.17)$$

where C_1 and C_2 are real constants. In (2.12) and (2.17), the factor $\eta_0 = \pm 1$ and the odderon trajectory function are unknown. We assume $\alpha_0(t) = 1 + \epsilon_0 + \alpha'_0 t$ with the parameters ϵ_0 and α'_0 that should be determined by experiment. Of course, the Pomeron amplitude must dominate over the odderon one for $s \rightarrow \infty$ in order to ensure positive total pp and $p\bar{p}$ cross sections. Thus, we must require $\epsilon_0 \leq \epsilon_{\mathbb{P}}$. For our study here, we assume $\beta_{\mathbb{O}pp} = 0.1 \times \beta_{\mathbb{P}pp} \simeq 0.2 \text{ GeV}^{-1}$, $\alpha'_0 = \alpha'_{\mathbb{P}}$, $\epsilon_0 = 0.0800$, $\eta_0 = -1$, and (C_1, C_2) as listed in (A10). How these parameters are determined from comparisons between theory and experiment will be discussed in Sec. IVA.

In the following, we use tensor-product notation. The first factors will always refer to the p_a - p_1 line, and the second refer to the p_b - p_2 line of the diagrams shown in Fig. 1.

In our model, the off-shell proton-proton scattering amplitude has the form

$$\begin{aligned} \mathcal{M}^{(0)}(p_a, p_b, p_1, p_2) &= \mathcal{M}_{\mathbb{P}}^{(0)} + \mathcal{M}_{f_{2R}}^{(0)} + \mathcal{M}_{a_{2R}}^{(0)} + \mathcal{M}_{\mathbb{O}}^{(0)} + \mathcal{M}_{\omega_R}^{(0)} + \mathcal{M}_{\rho_R}^{(0)} \\ &= i\mathcal{F}_T(s, t) \left[\gamma^\mu \otimes \gamma_\mu(p_a + p_1, p_b + p_2) + (\not{p}_b + \not{p}_2) \otimes (\not{p}_a + \not{p}_1) - \frac{1}{2} (\not{p}_a + \not{p}_1) \otimes (\not{p}_b + \not{p}_2) \right] \\ &\quad - \mathcal{F}_V(s, t) \gamma^\mu \otimes \gamma_\mu. \end{aligned} \quad (2.18)$$

With the helicities $\lambda_a, \lambda_b, \lambda_1, \lambda_2 \in \{-1/2, 1/2\}$, we get for the on-shell matrix element

$$\begin{aligned} &\langle p(p_1, \lambda_1), p(p_2, \lambda_2) | \mathcal{T} | p(p_a, \lambda_a), p(p_b, \lambda_b) \rangle \\ &\equiv \mathcal{M}^{(\text{on shell})pp}(s, t) \\ &= \bar{u}_1 \otimes \bar{u}_2 \mathcal{M}^{(0)}(p_a, p_b, p_1, p_2) u_a \otimes u_b |_{\text{on shell}} \\ &= i\mathcal{F}_T(s, t) [\bar{u}_1 \gamma^\mu u_a \bar{u}_2 \gamma_\mu u_b (p_a + p_1, p_b + p_2) + \bar{u}_1 \gamma^\mu u_a (p_b + p_2)_\mu \bar{u}_2 \gamma^\nu u_b (p_a + p_1)_\nu \\ &\quad - 2m_p^2 \bar{u}_1 u_a \bar{u}_2 u_b] - \mathcal{F}_V(s, t) \bar{u}_1 \gamma^\mu u_a \bar{u}_2 \gamma_\mu u_b. \end{aligned} \quad (2.19)$$

For brevity of notation, we define here and in the following for the spinors $u_a = u(p_a, \lambda_a)$, $\bar{u}_1 = \bar{u}(p_1, \lambda_1)$, etc. We also denote $\mathcal{M}^{(\text{on shell})pp}(s, t)$ as the on-shell pp elastic scattering amplitude.

We consider now the high-energy small-angle limit where we have the simple relations

$$\begin{aligned} \bar{u}(p_1, \lambda_1) \gamma^\mu u(p_a, \lambda_a) &\cong (p_a + p_1)^\mu \delta_{\lambda_1 \lambda_a}, \\ (p_a + p_1, p_b + p_2) &\cong 2s. \end{aligned} \quad (2.20)$$

From (2.19) we get, for $s \rightarrow \infty$, setting a possible odderon contribution to zero, the Pomeron contribution as leading term in the form

$$\mathcal{M}^{(\text{on shell})pp}(s, t) \rightarrow i8s^2 \mathcal{F}_{\mathbb{P}pp}(s, t) \delta_{\lambda_1 \lambda_a} \delta_{\lambda_2 \lambda_b}. \quad (2.21)$$

In this high-energy small-angle limit, the amplitude calculated from the tensor-Pomeron exchange is the same as the standard Donnachie-Landshoff amplitude; see the discussion in Chap. 6.1 of Ref. [28].

Coming back to the general case, we emphasize that in the following we use the exact formulas (2.18) and (2.19), without the approximations (2.20).

The total cross section for unpolarized protons, obtained from the forward-scattering amplitudes using the optical theorem, is

$$\begin{aligned}
\sigma_{\text{tot}}(pp) &= \frac{1}{\sqrt{s(s-4m_p^2)}} \frac{1}{4} \sum_{\lambda_a, \lambda_b} \text{Im} \langle p(p_a, \lambda_a), p(p_b, \lambda_b) | \mathcal{T} | p(p_a, \lambda_a), p(p_b, \lambda_b) \rangle \\
&= \frac{1}{\sqrt{s(s-4m_p^2)}} \{ \text{Re} \mathcal{F}_T(s, 0) 8[(s-2m_p^2)^2 - m_p^4] - \text{Im} \mathcal{F}_V(s, 0) 2(s-2m_p^2) \}.
\end{aligned} \tag{2.22}$$

With (2.9)–(2.17), this gives

$$\begin{aligned}
\sigma_{\text{tot}}(pp) &= 2 \left(1 - \frac{4m_p^2}{s} \right)^{-1/2} \left\{ \left[(3\beta_{pp})^2 (s\alpha'_{\mathbb{P}})^{\alpha_{\mathbb{P}}(0)-1} \cos\left(\frac{\pi}{2}(\alpha_{\mathbb{P}}(0)-1)\right) \right. \right. \\
&\quad + \left(\frac{g_{f_{2\mathbb{R}}pp}}{M_0} \right)^2 (s\alpha'_{f_{2\mathbb{R}}})^{\alpha_{f_{2\mathbb{R}}}(0)-1} \cos\left(\frac{\pi}{2}(\alpha_{f_{2\mathbb{R}}}(0)-1)\right) \\
&\quad + \left. \left(\frac{g_{a_{2\mathbb{R}}pp}}{M_0} \right)^2 (s\alpha'_{a_{2\mathbb{R}}})^{\alpha_{a_{2\mathbb{R}}}(0)-1} \cos\left(\frac{\pi}{2}(\alpha_{a_{2\mathbb{R}}}(0)-1)\right) \right] \left(1 - \frac{4m_p^2}{s} + \frac{3m_p^4}{s^2} \right) \right. \\
&\quad - \left[-\eta_{\mathbb{O}} (3\beta_{\mathbb{O}pp})^2 (s\alpha'_{\mathbb{O}})^{\alpha_{\mathbb{O}}(0)-1} \left[\cos\left(\frac{\pi}{2}\alpha_{\mathbb{O}}(0)\right) (C_1 + C_2 \ln(s\alpha'_{\mathbb{O}})) - C_2 \frac{\pi}{2} \sin\left(\frac{\pi}{2}\alpha_{\mathbb{O}}(0)\right) \right] \right. \\
&\quad + \left(\frac{g_{\omega_{\mathbb{R}}pp}}{M_-} \right)^2 (s\alpha'_{\omega_{\mathbb{R}}})^{\alpha_{\omega_{\mathbb{R}}}(0)-1} \cos\left(\frac{\pi}{2}\alpha_{\omega_{\mathbb{R}}}(0)\right) \\
&\quad + \left. \left. \left(\frac{g_{\rho_{\mathbb{R}}pp}}{M_-} \right)^2 (s\alpha'_{\rho_{\mathbb{R}}})^{\alpha_{\rho_{\mathbb{R}}}(0)-1} \cos\left(\frac{\pi}{2}\alpha_{\rho_{\mathbb{R}}}(0)\right) \right] \left(1 - \frac{2m_p^2}{s} \right) \right\}.
\end{aligned} \tag{2.23}$$

Here, we have used the expression (2.17) inserted into (2.16). To get the expression with (2.12) for the odderon exchange, we have to set $C_1 = 1$ and $C_2 = 0$.

B. Reaction $p\bar{p} \rightarrow p\bar{p}$

Here, we study the reaction (2.2), where p and \bar{p} can be on or off shell. In our model, considering only hadronic exchanges, we have the diagrams shown in Fig. 2. For high c.m. energies and small momentum transfers (2.7), the s -channel exchanges should be negligible.

Now, we get for the $p\bar{p}$ off-shell amplitude

$$\begin{aligned}
\mathcal{M}_{p\bar{p}}^{(0)}(p_a, p_b, p_1, p_2) &= i\mathcal{F}_T(s, t) \left[\gamma^\mu \otimes \gamma_\mu(p_a + p_1, p_b + p_2) + (\not{p}_b + \not{p}_2) \otimes (\not{p}_a + \not{p}_1) - \frac{1}{2} (\not{p}_a + \not{p}_1) \otimes (\not{p}_b + \not{p}_2) \right] \\
&\quad + \mathcal{F}_V(s, t) \gamma^\mu \otimes \gamma_\mu.
\end{aligned} \tag{2.24}$$

For the on-shell amplitude, we get

$$\begin{aligned}
\langle p(p_1, \lambda_1), \bar{p}(p_2, \lambda_2) | \mathcal{T} | p(p_a, \lambda_a), \bar{p}(p_b, \lambda_b) \rangle &= \bar{u}_1 \otimes \bar{v}_b \mathcal{M}_{p\bar{p}}^{(0)}(p_a, p_b, p_1, p_2) u_a \otimes v_2 \\
&= i\mathcal{F}_T(s, t) [\bar{u}_1 \gamma^\mu u_a \bar{v}_b \gamma_\mu v_2(p_a + p_1, p_b + p_2) + \bar{u}_1 \gamma^\mu u_a (p_b + p_2)_\mu \bar{v}_b \gamma^\nu v_2(p_a + p_1)_\nu + 2m_p^2 \bar{u}_1 u_a \bar{v}_b v_2] \\
&\quad + \mathcal{F}_V(s, t) \bar{u}_1 \gamma^\mu u_a \bar{v}_b \gamma_\mu v_2.
\end{aligned} \tag{2.25}$$

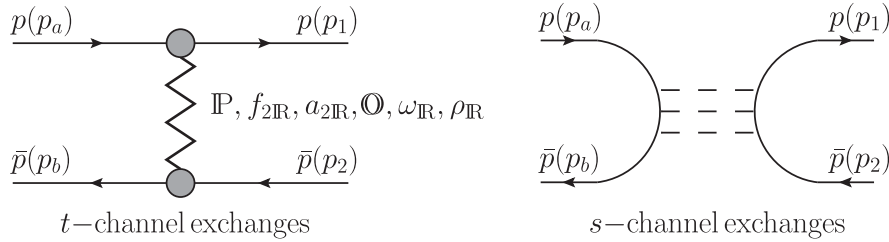


FIG. 2. The diagrams for $p\bar{p} \rightarrow p\bar{p}$ elastic scattering with the t - and s -channel exchanges.

The total $p\bar{p}$ cross section is

$$\begin{aligned}\sigma_{\text{tot}}(p\bar{p}) &= \frac{1}{\sqrt{s(s-4m_p^2)}} \frac{1}{4} \sum_{\lambda_a, \lambda_b} \text{Im} \langle p(p_a, \lambda_a), \bar{p}(p_b, \lambda_b) | T | p(p_a, \lambda_a), \bar{p}(p_b, \lambda_b) \rangle \\ &= \frac{1}{\sqrt{s(s-4m_p^2)}} \{ \text{Re} \mathcal{F}_T(s, 0) 8[(s-2m_p^2)^2 - m_p^4] + \text{Im} \mathcal{F}_V(s, 0) 2(s-2m_p^2) \}.\end{aligned}\quad (2.26)$$

With (2.9)–(2.17), this gives

$$\begin{aligned}\sigma_{\text{tot}}(p\bar{p}) &= 2 \left(1 - \frac{4m_p^2}{s}\right)^{-1/2} \left\{ \left[(3\beta_{\mathbb{P}pp})^2 (s\alpha'_{\mathbb{P}})^{\alpha_{\mathbb{P}}(0)-1} \cos\left(\frac{\pi}{2}(\alpha_{\mathbb{P}}(0) - 1)\right) \right. \right. \\ &\quad + \left. \left(\frac{g_{f_{2\mathbb{R}}pp}}{M_0} \right)^2 (s\alpha'_{f_{2\mathbb{R}}})^{\alpha_{f_{2\mathbb{R}}}(0)-1} \cos\left(\frac{\pi}{2}(\alpha_{f_{2\mathbb{R}}}(0) - 1)\right) \right. \\ &\quad + \left. \left. \left(\frac{g_{a_{2\mathbb{R}}pp}}{M_0} \right)^2 (s\alpha'_{a_{2\mathbb{R}}})^{\alpha_{a_{2\mathbb{R}}}(0)-1} \cos\left(\frac{\pi}{2}(\alpha_{a_{2\mathbb{R}}}(0) - 1)\right) \right] \left(1 - \frac{4m_p^2}{s} + \frac{3m_p^4}{s^2}\right) \right. \\ &\quad + \left. \left[-\eta_{\mathbb{O}} (3\beta_{\mathbb{O}pp})^2 (s\alpha'_{\mathbb{O}})^{\alpha_{\mathbb{O}}(0)-1} \left[\cos\left(\frac{\pi}{2}\alpha_{\mathbb{O}}(0)\right) (C_1 + C_2 \ln(s\alpha'_{\mathbb{O}})) - C_2 \frac{\pi}{2} \sin\left(\frac{\pi}{2}\alpha_{\mathbb{O}}(0)\right) \right] \right. \right. \\ &\quad + \left. \left(\frac{g_{\omega_{\mathbb{R}}pp}}{M_-} \right)^2 (s\alpha'_{\omega_{\mathbb{R}}})^{\alpha_{\omega_{\mathbb{R}}}(0)-1} \cos\left(\frac{\pi}{2}\alpha_{\omega_{\mathbb{R}}}(0)\right) \right. \\ &\quad + \left. \left. \left(\frac{g_{\rho_{\mathbb{R}}pp}}{M_-} \right)^2 (s\alpha'_{\rho_{\mathbb{R}}})^{\alpha_{\rho_{\mathbb{R}}}(0)-1} \cos\left(\frac{\pi}{2}\alpha_{\rho_{\mathbb{R}}}(0)\right) \right] \left(1 - \frac{2m_p^2}{s}\right) \right\}.\end{aligned}\quad (2.27)$$

Comparing Eq. (2.18) with Eq. (2.24), Eq. (2.19) with Eq. (2.25), and Eq. (2.23) with Eq. (2.27), we see that for pp and $p\bar{p}$ scattering the $C = +1$ exchanges contribute with the same sign and the $C = -1$ exchanges contribute with opposite sign, as they should.

C. Reaction $pp \rightarrow pp\gamma$

Now, we consider the reaction (2.3). Here, we have the energy-momentum relation (2.5). The kinematic variables are

$$\begin{aligned}s &= (p_a + p_b)^2 = (p'_1 + p'_2 + k)^2, \\ s' &= (p_a + p_b - k)^2 = (p'_1 + p'_2)^2, \\ t_1 &= (p_a - p'_1)^2 = (p_b - p'_2 - k)^2, \\ t_2 &= (p_b - p'_2)^2 = (p_a - p'_1 - k)^2.\end{aligned}\quad (2.28)$$

For the photon emission process (2.3), we have seven types of diagrams shown in Fig. 3. In the diagrams (a), (b), (d), and (e), the photon is emitted from the external proton lines. The diagrams (c) and (f) correspond to contact terms. The precise definition of the contact terms and of the “structure” term (g) will be given below. For high c.m. energies \sqrt{s} and small momentum transfers $|t_{1,2}|$ [see (2.28)], the diagrams of Fig. 3 with $p'_1 \leftrightarrow p'_2$ are expected to give negligible contributions. We shall call the diagrams

(a), (b), (d), and (e), made gauge invariant by the addition of (c) and (f), the bremsstrahlung diagrams.

The relevant \mathcal{T} -matrix element is

$$\begin{aligned}\langle p(p'_1, \lambda_1), p(p'_2, \lambda_2), \gamma(k, \epsilon) | T | p(p_a, \lambda_a), p(p_b, \lambda_b) \rangle \\ = (\epsilon^\mu)^* \mathcal{M}_\mu^{(\text{total})}(p_a, \lambda_a; p_b, \lambda_b; p'_1, \lambda_1; p'_2, \lambda_2; k).\end{aligned}\quad (2.29)$$

We consider $\mathcal{M}_\mu^{(\text{total})}$ for arbitrary k . Gauge invariance requires

$$k^\mu \mathcal{M}_\mu^{(\text{total})} = 0.\quad (2.30)$$

Let the sum of the diagrams of Fig. 3 with \mathbb{P} and all other exchanges be

$$\begin{aligned}\mathcal{M}_\mu(p'_1, p'_2) &= \mathcal{M}_\mu^{(a)} + \mathcal{M}_\mu^{(b)} + \mathcal{M}_\mu^{(c)} + \mathcal{M}_\mu^{(d)} \\ &\quad + \mathcal{M}_\mu^{(e)} + \mathcal{M}_\mu^{(f)} + \mathcal{M}_\mu^{(g)}.\end{aligned}\quad (2.31)$$

The complete amplitude is then

$$\mathcal{M}_\mu^{(\text{total})} = \mathcal{M}_\mu(p'_1, p'_2) - \mathcal{M}_\mu(p'_2, p'_1),\quad (2.32)$$

where a corresponding exchange of helicities is understood. The relative minus sign here is due to the Fermi statistics, which requires the amplitude to be antisymmetric under interchange of the two final protons.

The inclusive cross section for the real-photon yield of the reaction (2.3), including a statistics factor 1/2 due to identical particles appearing in the final state, is as follows:

$$d\sigma(pp \rightarrow pp\gamma) = \frac{1}{2} \frac{1}{2\sqrt{s(s-4m_p^2)}} \frac{d^3k}{(2\pi)^3 2k^0} \int \frac{d^3p'_1}{(2\pi)^3 2p'_1{}^0} \frac{d^3p'_2}{(2\pi)^3 2p'_2{}^0} \times (2\pi)^4 \delta^{(4)}(p'_1 + p'_2 + k - p_a - p_b) \frac{1}{4} \sum_{p \text{ spins}} \mathcal{M}_\lambda^{(\text{total})} (\mathcal{M}_\rho^{(\text{total})})^* (-g^{\lambda\rho}). \quad (2.33)$$

Let, in the c.m. system, p'_{1z} and p'_{2z} be the momentum components of \mathbf{p}'_1 and \mathbf{p}'_2 in the direction of \mathbf{p}_a . Then, we can write (2.33) with (2.32) as

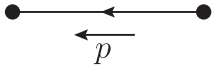
$$d\sigma(pp \rightarrow pp\gamma) = \frac{1}{2\sqrt{s(s-4m_p^2)}} \frac{d^3k}{(2\pi)^3 2k^0} \int \frac{d^3p'_1}{(2\pi)^3 2p'_1{}^0} \frac{d^3p'_2}{(2\pi)^3 2p'_2{}^0} \theta(p'_{1z} - p'_{2z}) (2\pi)^4 \delta^{(4)}(p'_1 + p'_2 + k - p_a - p_b) \times \frac{1}{4} \sum_{p \text{ spins}} (\mathcal{M}_\lambda(p'_1, p'_2) - \mathcal{M}_\lambda(p'_2, p'_1)) (\mathcal{M}_\rho(p'_1, p'_2) - \mathcal{M}_\rho(p'_2, p'_1))^* (-g^{\lambda\rho}). \quad (2.34)$$

We are interested in high c.m. energies \sqrt{s} and small momentum transfers. Then, for $p'_{1z} > p'_{2z}$, the amplitude $\mathcal{M}_\lambda(p'_2, p'_1)$ is very small and can be neglected. On the other hand, $\mathcal{M}_\lambda(p'_1, p'_2)$ is very small for $p'_{1z} < p'_{2z}$. Therefore, from (2.34), we get with very high accuracy

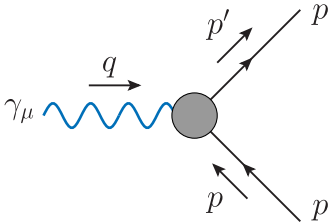
$$d\sigma(pp \rightarrow pp\gamma) = \frac{1}{2\sqrt{s(s-4m_p^2)}} \frac{d^3k}{(2\pi)^3 2k^0} \int \frac{d^3p'_1}{(2\pi)^3 2p'_1{}^0} \frac{d^3p'_2}{(2\pi)^3 2p'_2{}^0} \times (2\pi)^4 \delta^{(4)}(p'_1 + p'_2 + k - p_a - p_b) \frac{1}{4} \sum_{p \text{ spins}} \mathcal{M}_\lambda(p'_1, p'_2) (\mathcal{M}_\rho(p'_1, p'_2))^* (-g^{\lambda\rho}). \quad (2.35)$$

In the following, we shall, for brevity of notation, set $\mathcal{M}_\lambda \equiv \mathcal{M}_\lambda(p'_1, p'_2)$.

For calculating \mathcal{M}_λ from the diagrams of Fig. 3, we use the following standard proton propagator and γpp vertex:



$iS_F(p) = \frac{i}{\not{p} - m_p + i\epsilon} = i \frac{\not{p} + m_p}{p^2 - m_p^2 + i\epsilon}, \quad (2.36)$



$q = p' - p,$

$i\Gamma_\mu^{(\gamma pp)}(p', p) = -ie \left[\gamma_\mu + \frac{i}{2m_p} \sigma_{\mu\nu} q^\nu F_2(0) \right],$

$F_2(0) = \left(\frac{\mu_p}{\mu_N} - 1 \right), \quad \mu_N = \frac{e}{2m_p}, \quad \frac{\mu_p}{\mu_N} = 2.7928,$

$e > 0, \quad e = \sqrt{4\pi\alpha_{\text{em}}}.$

(2.37)

We take the form factors in (2.37) at $q^2 = 0$ in order to be consistent with the Ward-Takahashi identity [52,53]:

$$(p' - p)^\mu \Gamma_\mu^{(\gamma pp)}(p', p) = -e [S_F^{-1}(p') - S_F^{-1}(p)]. \quad (2.38)$$

In any case, we are finally interested in real photon emission where $k = -q$, $k^2 = q^2 = 0$.

Now, we list our results for the photon-bremsstrahlung amplitudes $\mathcal{M}_\mu^{(a)}, \dots, \mathcal{M}_\mu^{(f)}$ corresponding to the Pomeron-exchange diagrams (a)–(f) from Fig. 3 including the other exchanges $f_{2\mathbb{R}}, a_{2\mathbb{R}}, \omega_{\mathbb{R}}, \rho_{\mathbb{R}}, \mathbb{O}$.

With the off-shell pp elastic scattering amplitude (2.18), the standard proton propagator (2.36), and the γpp vertex function (2.37), we get the following radiative amplitudes:

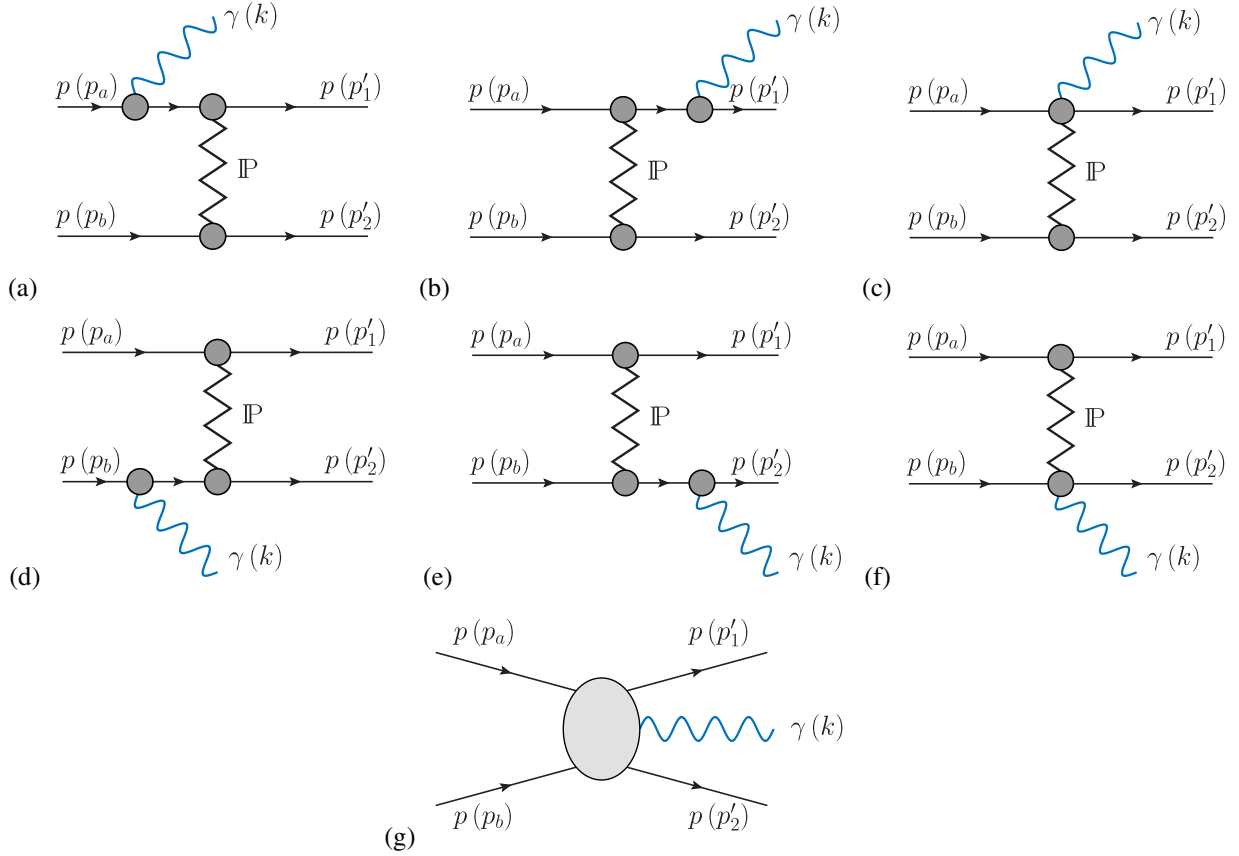


FIG. 3. Diagrams for the reaction $pp \rightarrow pp\gamma$ with exchange of the Pomeron \mathbb{P} (a–f) and the “structure” term (g). The diagrams for odderon and reggeon exchanges are as in parts a–f with \mathbb{P} replaced by $f_{2\mathbb{R}}$, $a_{2\mathbb{R}}$, \mathbb{O} , $\omega_{\mathbb{R}}$, and $\rho_{\mathbb{R}}$. In addition, there are the diagrams corresponding to the interchange of the two final protons $p(p'_1) \leftrightarrow p(p'_2)$. These are not shown here.

$$\begin{aligned}
\mathcal{M}_\mu^{(a)} &= -\bar{u}_{1'} \otimes \bar{u}_{2'} \mathcal{M}^{(0)}(p_a - k, p_b, p'_1, p'_2) (S_F(p_a - k) \Gamma_\mu^{(\gamma pp)}(p_a - k, p_a) u_a) \otimes u_b \\
&= e \bar{u}_{1'} \otimes \bar{u}_{2'} \left\{ i\mathcal{F}_T(s', t_2) \left[\gamma^\alpha \otimes \gamma_\alpha(p_a - k + p'_1, p_b + p'_2) + (\not{p}_b + \not{p}'_2) \otimes (\not{p}_a - \not{k} + \not{p}'_1) \right. \right. \\
&\quad \left. \left. - \frac{1}{2} (\not{p}_a - \not{k} + \not{p}'_1) \otimes (\not{p}_b + \not{p}'_2) \right] - \mathcal{F}_V(s', t_2) \gamma^\alpha \otimes \gamma_\alpha \right\} \\
&\quad \times \left[\frac{\not{p}_a - \not{k} + m_p}{(p_a - k)^2 - m_p^2 + i\epsilon} \left(\gamma_\mu - \frac{i}{2m_p} \sigma_{\mu\nu} k^\nu F_2(0) \right) u_a \right] \otimes u_b, \tag{2.39}
\end{aligned}$$

$$\begin{aligned}
\mathcal{M}_\mu^{(b)} &= -(\bar{u}_{1'} \Gamma_\mu^{(\gamma pp)}(p'_1, p'_1 + k) S_F(p'_1 + k)) \otimes \bar{u}_{2'} \mathcal{M}^{(0)}(p_a, p_b, p'_1 + k, p'_2) u_a \otimes u_b \\
&= e \left[\bar{u}_{1'} \left(\gamma_\mu - \frac{i}{2m_p} \sigma_{\mu\nu} k^\nu F_2(0) \right) \frac{\not{p}'_1 + \not{k} + m_p}{(p'_1 + k)^2 - m_p^2 + i\epsilon} \right] \otimes \bar{u}_{2'} \\
&\quad \times \left\{ i\mathcal{F}_T(s, t_2) \left[\gamma^\alpha \otimes \gamma_\alpha(p_a + p'_1 + k, p_b + p'_2) + (\not{p}_b + \not{p}'_2) \otimes (\not{p}_a + \not{p}'_1 + \not{k}) \right. \right. \\
&\quad \left. \left. - \frac{1}{2} (\not{p}_a + \not{p}'_1 + \not{k}) \otimes (\not{p}_b + \not{p}'_2) \right] - \mathcal{F}_V(s, t_2) \gamma^\alpha \otimes \gamma_\alpha \right\} u_a \otimes u_b. \tag{2.40}
\end{aligned}$$

Here, the functions \mathcal{F}_T and \mathcal{F}_V are defined in (2.15) and (2.16), respectively.

Using (2.38), we find

$$k^\mu \mathcal{M}_\mu^{(a)} = -e \bar{u}_{1'} \otimes \bar{u}_{2'} \mathcal{M}^{(0)}(p_a - k, p_b, p'_1, p'_2) u_a \otimes u_b, \tag{2.41}$$

$$k^\mu \mathcal{M}_\mu^{(b)} = e\bar{u}_{1'} \otimes \bar{u}_{2'} \mathcal{M}^{(0)}(p_a, p_b, p'_1 + k, p'_2) u_a \otimes u_b. \quad (2.42)$$

Now, we impose the gauge-invariance condition, which must hold also for the photon emission from the p_a - p'_1 lines in Fig. 3 alone:

$$k^\mu (\mathcal{M}_\mu^{(a)} + \mathcal{M}_\mu^{(b)} + \mathcal{M}_\mu^{(c)}) = 0. \quad (2.43)$$

We obtain then

$$\begin{aligned} k^\mu \mathcal{M}_\mu^{(c)} &= -k^\mu \mathcal{M}_\mu^{(a)} - k^\mu \mathcal{M}_\mu^{(b)} \\ &= e\bar{u}_{1'} \otimes \bar{u}_{2'} [\mathcal{M}^{(0)}(p_a - k, p_b, p'_1, p'_2) - \mathcal{M}^{(0)}(p_a, p_b, p'_1 + k, p'_2)] u_a \otimes u_b \\ &= e\bar{u}_{1'} \otimes \bar{u}_{2'} \left\{ i\mathcal{F}_T(s', t_2) \left[\gamma^\alpha \otimes \gamma_\alpha (p_a - k + p'_1, p_b + p'_2) + (\not{p}_b + \not{p}'_2) \otimes (\not{p}_a - \not{k} + \not{p}'_1) \right. \right. \\ &\quad \left. \left. - \frac{1}{2} (\not{p}_a - \not{k} + \not{p}'_1) \otimes (\not{p}_b + \not{p}'_2) \right] - \mathcal{F}_V(s', t_2) \gamma^\alpha \otimes \gamma_\alpha \right. \\ &\quad \left. - i\mathcal{F}_T(s, t_2) \left[\gamma^\alpha \otimes \gamma_\alpha (p_a + p'_1 + k, p_b + p'_2) + (\not{p}_b + \not{p}'_2) \otimes (\not{p}_a + \not{p}'_1 + \not{k}) \right. \right. \\ &\quad \left. \left. - \frac{1}{2} (\not{p}_a + \not{p}'_1 + \not{k}) \otimes (\not{p}_b + \not{p}'_2) \right] + \mathcal{F}_V(s, t_2) \gamma^\alpha \otimes \gamma_\alpha \right\} u_a \otimes u_b. \end{aligned} \quad (2.44)$$

We have from (2.28)

$$\begin{aligned} s' &= (p_a + p_b - k)^2 \\ &= (p_a + p_b)^2 - 2(k, p_a + p_b) + k^2 \\ &= s - (k, 2p_a + 2p_b - k) \end{aligned} \quad (2.45)$$

and define

$$\chi = \frac{(k, 2p_a + 2p_b - k)}{s}. \quad (2.46)$$

Now, using the expressions given by Eqs. (2.9)–(2.14), (2.45), and (2.46), we get

$$\mathcal{F}_{\mathbb{P}pp}(s', t_2) = \mathcal{F}_{\mathbb{P}pp}(s, t_2) [1 + \chi(2 - \alpha_{\mathbb{P}}(t_2))g_{\mathbb{P}}(\chi, t_2)], \quad (2.47)$$

$$g_{\mathbb{P}}(\chi, t_2) = \frac{1}{(2 - \alpha_{\mathbb{P}}(t_2))\chi} [(1 - \chi)^{\alpha_{\mathbb{P}}(t_2)-2} - 1], \quad (2.48)$$

and analogously for $f_{2\mathbb{R}}$ and $a_{2\mathbb{R}}$, and

$$\mathcal{F}_{\mathbb{O}pp}(s', t_2) = \mathcal{F}_{\mathbb{O}pp}(s, t_2) [1 + \chi(1 - \alpha_{\mathbb{O}}(t_2))g_{\mathbb{O}}(\chi, t_2)], \quad (2.49)$$

$$g_{\mathbb{O}}(\chi, t_2) = \frac{1}{(1 - \alpha_{\mathbb{O}}(t_2))\chi} [(1 - \chi)^{\alpha_{\mathbb{O}}(t_2)-1} - 1], \quad (2.50)$$

and analogously for $\omega_{\mathbb{R}}$ and $\rho_{\mathbb{R}}$.

From (2.47)–(2.50) and supplementing with the reggeons, we get

$$\mathcal{F}_T(s', t) = \mathcal{F}_T(s, t) + \chi \Delta \mathcal{F}_T(s, t, \chi), \quad (2.51)$$

$$\mathcal{F}_V(s', t) = \mathcal{F}_V(s, t) + \chi \Delta \mathcal{F}_V(s, t, \chi), \quad (2.52)$$

where

$$\begin{aligned} \Delta \mathcal{F}_T(s, t, \chi) &= (2 - \alpha_{\mathbb{P}}(t))g_{\mathbb{P}}(\chi, t)\mathcal{F}_{\mathbb{P}pp}(s, t) + (2 - \alpha_{f_{2\mathbb{R}}}(t))g_{f_{2\mathbb{R}}}(\chi, t)\mathcal{F}_{f_{2\mathbb{R}}pp}(s, t) \\ &\quad + (2 - \alpha_{a_{2\mathbb{R}}}(t))g_{a_{2\mathbb{R}}}(\chi, t)\mathcal{F}_{a_{2\mathbb{R}}pp}(s, t), \end{aligned} \quad (2.53)$$

$$\begin{aligned} \Delta \mathcal{F}_V(s, t, \chi) &= (1 - \alpha_{\mathbb{O}}(t))g_{\mathbb{O}}(\chi, t)\mathcal{F}_{\mathbb{O}pp}(s, t) + (1 - \alpha_{\omega_{\mathbb{R}}}(t))g_{\omega_{\mathbb{R}}}(\chi, t)\mathcal{F}_{\omega_{\mathbb{R}}pp}(s, t) \\ &\quad + (1 - \alpha_{\rho_{\mathbb{R}}}(t))g_{\rho_{\mathbb{R}}}(\chi, t)\mathcal{F}_{\rho_{\mathbb{R}}pp}(s, t). \end{aligned} \quad (2.54)$$

The formulas for the odderon in (2.49), (2.50), and (2.54) apply for a single-pole odderon (2.12), (A7). The corresponding formulas for a double-pole odderon (2.17), (A9) are given in Appendix A; see (A24)–(A26).

Inserting all this in (2.44), we get

$$\begin{aligned}
k^\mu \mathcal{M}_\mu^{(c)} = e \bar{u}_{1'} \otimes \bar{u}_{2'} \left\{ -i \mathcal{F}_T(s, t_2) [2\gamma^\alpha \otimes \gamma_\alpha(k, p_b + p_2') + 2(\not{p}_b + \not{p}_2') \otimes \not{k} - \not{k} \otimes (\not{p}_b + \not{p}_2')] \right. \\
+ i \frac{(k, 2p_a + 2p_b - k)}{s} \Delta \mathcal{F}_T(s, t_2, \kappa) \\
\times \left[\gamma^\alpha \otimes \gamma_\alpha(p_a + p_1' - k, p_b + p_2') + (\not{p}_b + \not{p}_2') \otimes (\not{p}_a + \not{p}_1' - \not{k}) - \frac{1}{2} (\not{p}_a + \not{p}_1' - \not{k}) \otimes (\not{p}_b + \not{p}_2') \right] \\
\left. - \frac{(k, 2p_a + 2p_b - k)}{s} \Delta \mathcal{F}_V(s, t_2, \kappa) \gamma^\alpha \otimes \gamma_\alpha \right\} u_a \otimes u_b. \quad (2.55)
\end{aligned}$$

Hence, the simplest solution of (2.55) for $\mathcal{M}_\mu^{(c)}$ has the form

$$\begin{aligned}
\mathcal{M}_\mu^{(c)} = e \bar{u}_{1'} \otimes \bar{u}_{2'} \left\{ -i \mathcal{F}_T(s, t_2) [2\gamma^\alpha \otimes \gamma_\alpha(p_b + p_2')_\mu + 2(\not{p}_b + \not{p}_2') \otimes \gamma_\mu - \gamma_\mu \otimes (\not{p}_b + \not{p}_2')] \right. \\
+ i \frac{(2p_a + 2p_b - k)_\mu}{s} \Delta \mathcal{F}_T(s, t_2, \kappa) \\
\times \left[\gamma^\alpha \otimes \gamma_\alpha(p_a + p_1' - k, p_b + p_2') + (\not{p}_b + \not{p}_2') \otimes (\not{p}_a + \not{p}_1' - \not{k}) - \frac{1}{2} (\not{p}_a + \not{p}_1' - \not{k}) \otimes (\not{p}_b + \not{p}_2') \right] \\
\left. - \frac{(2p_a + 2p_b - k)_\mu}{s} \Delta \mathcal{F}_V(s, t_2, \kappa) \gamma^\alpha \otimes \gamma_\alpha \right\} u_a \otimes u_b. \quad (2.56)
\end{aligned}$$

We define (2.56) as $\mathcal{M}_\mu^{(c)}$. Possible additions to this solution of the form

$$\tilde{\mathcal{M}}_\mu, \quad k^\mu \tilde{\mathcal{M}}_\mu = 0 \quad (2.57)$$

can and will be considered as a part of $\mathcal{M}_\mu^{(g)}$ for which we require

$$k^\mu \mathcal{M}_\mu^{(g)} = 0. \quad (2.58)$$

For the diagrams (d), (e), and (f), we get

$$\mathcal{M}_\mu^{(d)} = \mathcal{M}_\mu^{(a)} \Big|_{\substack{(p_a, \lambda_a) \leftrightarrow (p_b, \lambda_b) \\ (p_1', \lambda_1) \leftrightarrow (p_2', \lambda_2)}}, \quad (2.59)$$

$$\mathcal{M}_\mu^{(e)} = \mathcal{M}_\mu^{(b)} \Big|_{\substack{(p_a, \lambda_a) \leftrightarrow (p_b, \lambda_b) \\ (p_1', \lambda_1) \leftrightarrow (p_2', \lambda_2)}}, \quad (2.60)$$

$$\mathcal{M}_\mu^{(f)} = \mathcal{M}_\mu^{(c)} \Big|_{\substack{(p_a, \lambda_a) \leftrightarrow (p_b, \lambda_b) \\ (p_1', \lambda_1) \leftrightarrow (p_2', \lambda_2)}}. \quad (2.61)$$

With the exchanges $(p_a, \lambda_a) \leftrightarrow (p_b, \lambda_b)$ and $(p_1', \lambda_1) \leftrightarrow (p_2', \lambda_2)$, we shall also exchange the order of the factors in the tensor products. In this way, the first factors in the tensor products always refer to the $p_a - p_1'$ line, and the second factors refer to the $p_b - p_2'$ line, in the diagrams of Fig. 3.

We shall call

$$\mathcal{M}_\mu^{(\text{standard})} = \mathcal{M}_\mu^{(a)} + \mathcal{M}_\mu^{(b)} + \mathcal{M}_\mu^{(c)} + \mathcal{M}_\mu^{(d)} + \mathcal{M}_\mu^{(e)} + \mathcal{M}_\mu^{(f)} \quad (2.62)$$

our standard, or ‘‘conventional,’’ amplitude. We have by construction

$$k^\mu \mathcal{M}_\mu^{(\text{standard})} = 0. \quad (2.63)$$

All ‘‘anomalous’’ terms are then subsumed in $\mathcal{M}_\mu^{(g)}$, which satisfies (2.58) and has no singularity for $k_\mu \rightarrow 0$.

The explicit forms of the amplitudes $\mathcal{M}_\mu^{(a)}, \dots, \mathcal{M}_\mu^{(f)}$ in (2.39), (2.40), (2.56), and (2.59)–(2.61), calculated in the tensor-Pomeron approach, are a main result of our present paper. But it turns out that these forms are not very convenient for numerical computations. Therefore, in Appendix B, we rewrite these amplitudes in a different form, which is more easy to handle numerically.

The intermediate protons in the diagrams of Fig. 3 (a, b, d, e) are off shell, and in principle we should take care of that fact in our model. But at present, we set possible cutoff form factors for off-shell protons in the Pomeron-proton and photon-proton vertices and in the proton propagator to 1. Note that a naive usage of form factors can violate the

Ward-Takahashi identity (2.38). We expect, however, that in our regions of interest, in the small k_\perp and ω ranges and especially in the soft-photon limit, the off-shell effects should be small.

III. SOFT-PHOTON APPROXIMATION APPROACH

In the following, we shall compare our exact model results, which we shall call standard results, for the amplitude (2.62), using (B3)–(B16), to two soft-photon approximations: SPA1 and SPA2. In these SPAs, we consider only the Pomeron-exchange terms for the radiative amplitudes $\mathcal{M}_\mu^{(a)}, \dots, \mathcal{M}_\mu^{(f)}$ in (2.62). Below, we list the explicit expressions for real photon emission in pp scattering:

SPA1.—Here, we keep only the pole terms $\propto \omega^{-1}$ for $\mathcal{M}_\mu^{(a)}, \dots, \mathcal{M}_\mu^{(f)}$ in (2.62). For real photons ($k^2 = 0$), neglecting gauge terms $\propto k_\mu$, and with $p'_1 \rightarrow p_1$, $p'_2 \rightarrow p_2$, we get

$$\begin{aligned} \mathcal{M}_\mu \rightarrow \mathcal{M}_{\mu, \text{SPA1}} &= e \mathcal{M}^{(\text{on shell})pp}(s, t) \\ &\times \left[-\frac{P_{a\mu}}{(p_a \cdot k)} + \frac{P_{1\mu}}{(p_1 \cdot k)} - \frac{P_{b\mu}}{(p_b \cdot k)} + \frac{P_{2\mu}}{(p_2 \cdot k)} \right]. \end{aligned} \quad (3.1)$$

Here, $\mathcal{M}^{(\text{on shell})pp}(s, t)$ is the on-shell pp -scattering amplitude given by (2.19). The result (3.1) is easily obtained from (B3), (B4), and (B15). Inserting (3.1) into (2.35), we get the following SPA1 result for the inclusive photon cross section where, for consistency, we neglect the photon momentum k in the energy-momentum conserving $\delta^{(4)}(\cdot)$ function:

$$\begin{aligned} d\sigma(pp \rightarrow pp\gamma)_{\text{SPA1}} &= \frac{d^3k}{(2\pi)^3 2k^0} \int d^3p_1 d^3p_2 e^2 \frac{d\sigma(pp \rightarrow pp)}{d^3p_1 d^3p_2} \\ &\times \left[-\frac{P_{a\mu}}{(p_a \cdot k)} + \frac{P_{1\mu}}{(p_1 \cdot k)} - \frac{P_{b\mu}}{(p_b \cdot k)} + \frac{P_{2\mu}}{(p_2 \cdot k)} \right] \\ &\times \left[-\frac{P_{a\nu}}{(p_a \cdot k)} + \frac{P_{1\nu}}{(p_1 \cdot k)} - \frac{P_{b\nu}}{(p_b \cdot k)} + \frac{P_{2\nu}}{(p_2 \cdot k)} \right] \\ &\times (-g^{\mu\nu}). \end{aligned} \quad (3.2)$$

Here,

$$\begin{aligned} \frac{d\sigma(pp \rightarrow pp)}{d^3p_1 d^3p_2} &= \frac{1}{2\sqrt{s(s-4m_p^2)}} \frac{1}{(2\pi)^3 2p_1^0 (2\pi)^3 2p_2^0} \\ &\times (2\pi)^4 \delta^{(4)}(p_1 + p_2 - p_a - p_b) \\ &\times \frac{1}{4} \sum_{p \text{ spins}} |\mathcal{M}^{(\text{on shell})pp}(s, t)|^2. \end{aligned} \quad (3.3)$$

In (3.2) and (3.3), we have a frequently used SPA. One takes the momentum distribution of the particles without radiation [see (3.3)] and multiplies it with the square of the emission factor in the square brackets in (3.1).

SPA2.—Here, we keep the energy-momentum relation (2.5). We consider again real photon emission and make in (2.35) the replacement

$$\mathcal{M}_\mu \rightarrow \mathcal{M}_{\mu, \text{SPA2}} = \mathcal{M}_{\mathbb{P}, \mu}^{(a+b+c)1} + \mathcal{M}_{\mathbb{P}, \mu}^{(d+e+f)1}. \quad (3.4)$$

The amplitude (3.4) corresponds to that given in (B4) plus (B15), taking only the Pomeron exchange into account. Here, the squared momentum transfer is t_2 for the diagrams of Figs. 3(a)–3(c) and t_1 for those of Figs. 3(d)–3(f), where t_1 and t_2 are defined in (2.28). Also, in the calculation of the photon distributions, we keep the correct energy-momentum conserving $\delta^{(4)}(\cdot)$ function in (2.35).

We also consider a slightly modified SPA1 amplitude where we use the high-energy small-angle limit relations (2.20). We get then $\hat{\mathcal{M}}_{\mu, \text{SPA1}}$ as in (3.1) but with (2.21) inserted for $\mathcal{M}^{(\text{on shell})pp}$:

$$\begin{aligned} \hat{\mathcal{M}}_{\mu, \text{SPA1}} &= ie8s^2 \mathcal{F}_{\mathbb{P}pp}(s, t) \delta_{\lambda_1 \lambda_a} \delta_{\lambda_2 \lambda_b} \\ &\times \left[-\frac{P_{a\mu}}{(p_a \cdot k)} + \frac{P_{1\mu}}{(p_1 \cdot k)} - \frac{P_{b\mu}}{(p_b \cdot k)} + \frac{P_{2\mu}}{(p_2 \cdot k)} \right]. \end{aligned} \quad (3.5)$$

For the SPA2, we examine, furthermore, the approximation

$$\begin{aligned} \hat{\mathcal{M}}_{\mu, \text{SPA2}} &= ie8s^2 \mathcal{F}_{\mathbb{P}pp}(s, t_2) \delta_{\lambda_1 \lambda_a} \delta_{\lambda_2 \lambda_b} \left[-\frac{P_{a\mu}}{(p_a \cdot k)} + \frac{P'_{1\mu}}{(p'_1 \cdot k)} \right] \\ &+ ie8s^2 \mathcal{F}_{\mathbb{P}pp}(s, t_1) \delta_{\lambda_1 \lambda_a} \delta_{\lambda_2 \lambda_b} \\ &\times \left[-\frac{P_{b\mu}}{(p_b \cdot k)} + \frac{P'_{2\mu}}{(p'_2 \cdot k)} \right]. \end{aligned} \quad (3.6)$$

How these approximations (3.5) and (3.6) agree with $\mathcal{M}_{\mu, \text{SPA1}}$ from the formula (3.1) and $\mathcal{M}_{\mu, \text{SPA2}}$ from the formula (3.4) will be discussed at the end of Sec. IV B.

IV. RESULTS

Below, we show our results for total and elastic pp and $p\bar{p}$ scattering (Sec. IV A) and results for the $pp \rightarrow pp\gamma$ reaction from the bremsstrahlung mechanism (Sec. IV B).

A. Comparison of the model results with the total and elastic pp and $p\bar{p}$ cross section data

Here, we compare our results obtained from Eqs. (2.19) and (2.25) to the experimental data for σ_{tot} , $d\sigma/dt$, and ρ , that is, the ratio of the real part to imaginary part of the forward scattering amplitude,

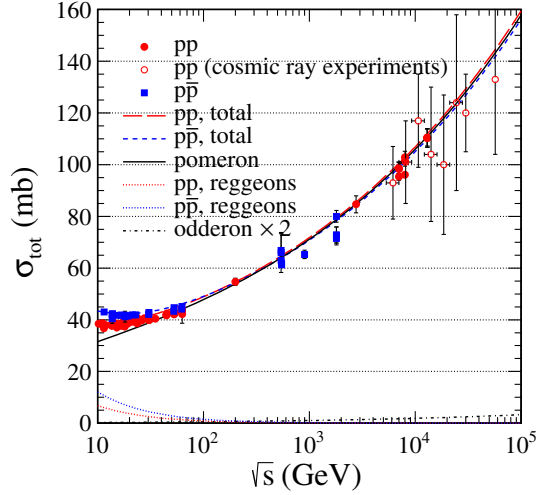


FIG. 4. The total cross sections for pp and $p\bar{p}$ scattering as a function of the center-of-mass energy \sqrt{s} . The red long-dashed line and the blue dashed line correspond to our complete results for pp and $p\bar{p}$ scattering, respectively. Here, the Pomeron parameters are as in (A1), (A2), (A11), and (A12) with $\epsilon_{\mathbb{P}} = 0.0865$. The reggeon parameters are given in (A3)–(A6), and we take here for the odderon the parameters (A9), (A10), and (A23), with $(C_1, C_2) = (-2.0, 0.3)$. The black solid line corresponds to the Pomeron exchange alone, the dotted lines correspond to the reggeon exchanges (lower for pp , upper for $p\bar{p}$), and the dot-dashed line corresponds to the odderon contribution increased by a factor of 2 for visualization. The experimental data are from Ref. [62], from Eq. (8) and Figs. 4 and 5 of Ref. [63], from Ref. [64], and from the Particle Data Group [65] (see Ref. [66]).

$$\rho = \frac{\text{Re}T(s, 0)}{\text{Im}T(s, 0)}. \quad (4.1)$$

We emphasize that in the present paper it is *not* our purpose to perform a precision fit to the available experimental data on these quantities, say, from ISR to LHC energies. Here ISR means the CERN Intersecting Storage Rings which operated with a maximum c.m. energy of 63 GeV. Such fits have been, for instance, given in Refs. [54–61]. Our aim here is to obtain a reasonable description of the data mainly at $\sqrt{s} = 13$ TeV. We want to fix the parameters of our model in this way. The *main* aim of our paper is to give then predictions for soft-photon radiation in proton-proton elastic collisions for the LHC energy range; see Sec. IV B.

In Fig. 4, we present the total pp (see the red points and lines) and $p\bar{p}$ (see the blue points and lines) cross sections for $\sqrt{s} > 10$ GeV. We show our complete theoretical results including the Pomeron, the reggeon, and the odderon exchanges and their separate contributions. First, we notice that, of course, the high-energy cross sections are dominated by the Pomeron exchange (see the black solid line). The cross sections with the Pomeron contribution alone are $\sigma_{\text{tot}}(pp) = 102.0$ mb for $\sqrt{s} = 8$ TeV and $\sigma_{\text{tot}}(pp) = 110.9$ mb for $\sqrt{s} = 13$ TeV. For the odderon exchange, we use the double-pole Ansatz (A9) with the

parameters (A10) and $(C_1, C_2) = (-2.0, 0.3)$ adjusted to describe $\rho = 0.1$ found by TOTEM at $\sqrt{s} = 13$ TeV. See the discussion below in connection with Fig. 6 which presents ρ as function of \sqrt{s} . There we also show the results for two more values $(C_1, C_2) = (-1.0, 0.1)$ and $(-1.5, 0.2)$. These lead to values of $\rho > 0.1$ at $\sqrt{s} = 13$ TeV. Here, we are interested in the total cross sections where the odderon effects are very small. We get, for instance, for the two cases $(C_1, C_2) = (-1.0, 0.1)$ and $(-2.0, 0.3)$ the total cross sections, $\sigma_{\text{tot}}(pp) = 102.2$ and 102.9 mb for $\sqrt{s} = 8$ TeV and $\sigma_{\text{tot}}(pp) = 111.2$ and 111.9 mb for $\sqrt{s} = 13$ TeV, respectively. Our results are in good agreement with the TOTEM results: $\sigma_{\text{tot}}(pp)|_{\text{exp}} = (102.9 \pm 2.3)$ mb and $\sigma_{\text{tot}}(pp)|_{\text{exp}} = (103.0 \pm 2.3)$ mb for $\sqrt{s} = 8$ TeV [62] and $\sigma_{\text{tot}}(pp)|_{\text{exp}} = (110.6 \pm 3.4)$ mb [63] and $\sigma_{\text{tot}}(pp)|_{\text{exp}} = (110.3 \pm 3.5)$ mb [64] for $\sqrt{s} = 13$ TeV.¹ Note that we get for large energies a total cross section for pp exceeding that for $p\bar{p}$ collisions, $\sigma_{\text{tot}}(pp) > \sigma_{\text{tot}}(p\bar{p})$.

In Fig. 5, we show the pp elastic differential cross sections for our model and the TOTEM data [64,67] measured at $\sqrt{s} = 13$ TeV. We find a quite good description of the data in the region $0.003 \text{ GeV}^2 \leq -t \leq 0.26 \text{ GeV}^2$ taking $\epsilon_{\mathbb{P}} = 0.0865$ and assuming the form factor $F(t) = \exp(-b|t|)$ with only one parameter, $b = 2.95 \text{ GeV}^{-2}$. For comparison, we show also the results for $\epsilon_{\mathbb{P}} = 0.0808$ and the Dirac form factor $F_1(t)$. We should not expect our single-Pomeron exchange model to give a precision fit for $d\sigma/dt$ in the diffractive dip region and beyond. The common lore is that in order to produce the dip one needs the interference of various terms in the amplitude, at least three terms: $\mathbb{P} + \mathbb{P}\mathbb{P} + ggg$; see, e.g., Refs. [48,54]. In Refs. [55,56], the authors discussed the so-called break effect, which leads to a smooth deflection of the linear exponential behavior of the diffraction cone observed near $t = -0.1 \text{ GeV}^2$. The effect is related to the basic analytic properties of the theory (t -channel unitarity) and reflects the presence of the pion cloud around the nucleon. This small, but interesting, effect could easily be included in our parametrization of the t dependence of the pp elastic cross section. But, as mentioned above, for our purposes, we only need a reasonable description of the pp scattering data for $\sqrt{s} = 13$ TeV. And, as we show in Fig. 5, we obtain such a description in the t range of interest for us with our single-exponential form factor $F(t)$.

In Fig. 6, we show our results for ρ for the two elastic scattering processes pp and $p\bar{p}$ together with the experimental data. The solid lines represent results of our model without the odderon contribution. The Pomeron and reggeon parameters are the same as in Fig. 4. In the left

¹The cross sections $\sigma_{\text{tot}}(pp)|_{\text{exp}}$ from Refs. [63,64] for $\sqrt{s} = 13$ TeV were determined in a completely independent way and, therefore, were combined for uncertainty reduction. The result is then $\sigma_{\text{tot}}(pp)|_{\text{exp}} = (110.5 \pm 2.4)$ mb; see Eq. (21) of Ref. [64].

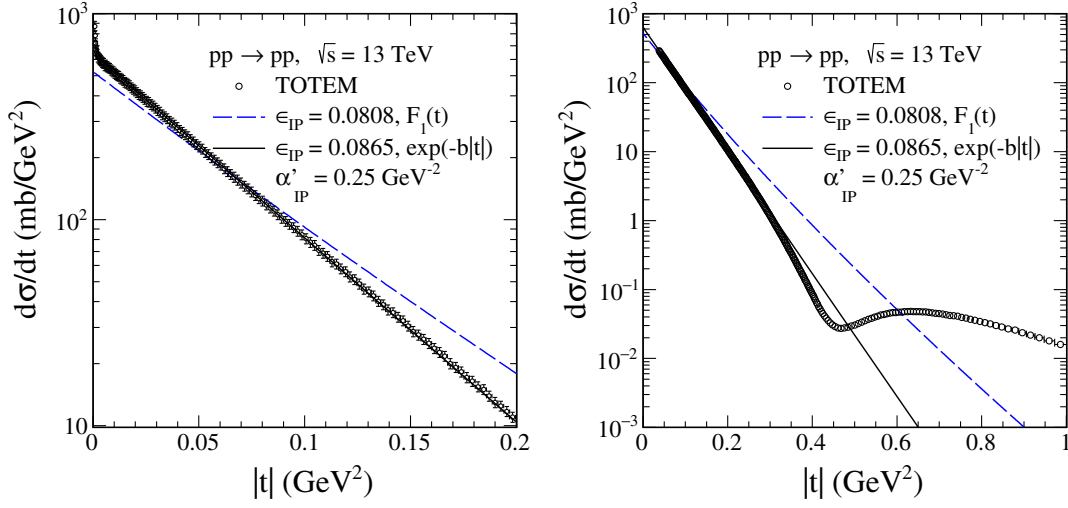


FIG. 5. The differential $pp \rightarrow pp$ cross sections measured by the TOTEM experiments at $\sqrt{s} = 13$ TeV [64,67]. We show our theoretical results obtained with two different Pomeron parameter sets: 1) $\epsilon_{\text{IP}} = 0.0808$ and the Dirac form factor $F_1(t)$ (see the blue dashed lines) and 2) $\epsilon_{\text{IP}} = 0.0865$ and the exponential form factor $F(t) = \exp(-b|t|)$ with $b = 2.95$ GeV^{-2} (see the black solid lines). In both cases, we take $\alpha'_{\text{IP}} = 0.25$ GeV^{-2} from (A2). Here, reggeon and odderon contributions are set to zero.

panel, the dashed and dotted lines show the results with the odderon exchange for different values of (C_1, C_2) in (2.17) and with the parameters (A10), (A23). The $C = -1$ reggeons lead to a splitting of the pp and $p\bar{p}$ results at smaller energies, while the odderon mainly affects the higher energies. The odderon parameters (C_1, C_2) are in essence determined by the ρ value at $\sqrt{s} = 13$ TeV. The values $\rho = 0.103, 0.116$, and 0.129 lead to $(C_1, C_2) = (-2.0, 0.3), (-1.5, 0.2)$, and $(-1.0, 0.1)$, respectively. In the right panel of Fig. 6, we show the results for $(C_1, C_2) = (-2.0, 0.3)$ and for $\epsilon_0 = 0$ and 0.05 to compare with

$\epsilon_0 = 0.08$. We can see that the ρ values mentioned can also be obtained by changing ϵ_0 .

The TOTEM Collaboration has reported direct measurements of the ρ parameter (4.1) through the Coulomb-nuclear interference in the very small $|t|$ region. The TOTEM results for ρ extracted from the data on the proton-proton differential cross section are:

- (i) $\rho = 0.12 \pm 0.03$ at $\sqrt{s} = 8$ TeV [62];
- (ii) $\rho = 0.09 \pm 0.01$ or $\rho = 0.10 \pm 0.01$ at $\sqrt{s} = 13$ TeV [64], depending on different physics assumptions and mathematical modelings.

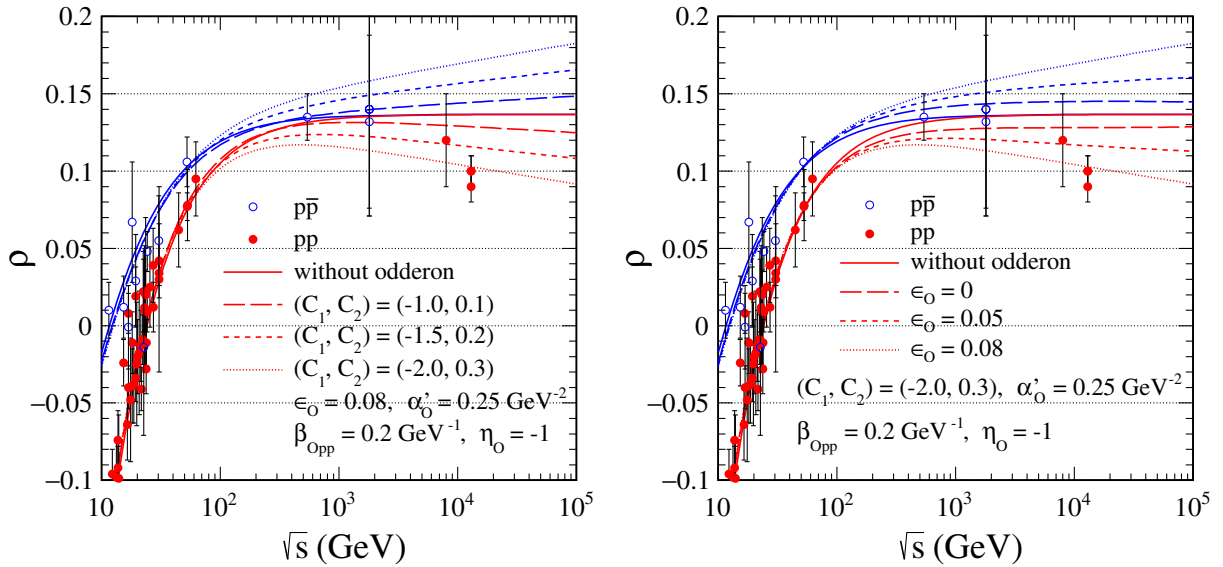


FIG. 6. Our results for the ρ parameter as function of the c.m. energy \sqrt{s} for $p\bar{p}$ (the blue upper lines) and pp (the red lower lines) scattering together with the experimental data from Refs. [62,64] and from Ref. [66]. Our complete results include \mathbb{P} , $f_{2\mathbb{R}}$, $a_{2\mathbb{R}}$, $\omega_{\mathbb{R}}$, $\rho_{\mathbb{R}}$, and \mathbb{O} exchanges. The solid lines are without the odderon contribution, and the dashed and dotted lines are with the odderon for different values of the parameters as described in the figure legends.

We can make the following statement. If we take the above ρ values from TOTEM as representing the truth, then, in the framework of our model, we need an odderon contribution at $t = 0$. Moreover, we could not find a reasonable description of the low- and high-energy data for ρ with a single-pole odderon. For these reasons, we consider here a double-pole odderon. To fit the TOTEM results for ρ , we have to choose the odderon parameters $(C_1, C_2) = (-2.0, 0.3)$. These findings are consistent with the results of Refs. [68,69]. These authors claim that a small value of ρ can be considered as the experimental discovery of the odderon for small $|t|$, namely, in its maximal form. The odderon was first introduced on theoretical grounds in Ref. [70]. For a review of odderon physics, we refer the reader to Ref. [71]. However, recent reanalyses of the TOTEM results [72,73] have shown that the values of ρ may be larger than those reported by the TOTEM Collaboration. For illustration, in Ref. [72], one finds $\rho \simeq 0.135$ at $\sqrt{s} = 8$ TeV and $\rho \simeq 0.133$ at $\sqrt{s} = 13$ TeV. Reference [73] gives $\rho = 0.123 \pm 0.010$ at $\sqrt{s} = 13$ TeV. To be consistent with these values, we should take in our model $(C_1, C_2) = (-1.0, 0.1)$.

In view of these ongoing discussions in the literature, we think that the low value $\rho = 0.1$ at $\sqrt{s} = 13$ TeV reported by TOTEM probably does not prove that there is an odderon contribution at $t = 0$; see, for instance, Refs. [74,75]. However, there are good reasons to believe that there is an odderon effect at larger $|t|$ (in the dip-bump region) that leads to a very significant difference between the differential cross sections of elastic pp and $p\bar{p}$ scattering, as was first seen at the CERN ISR at $\sqrt{s} = 53$ GeV [76]. Remarkably, such a difference had been predicted theoretically in Ref. [48]. The advantage of corresponding measurements at higher energies, e.g., at the LHC, is that subleading reggeon exchanges are very small there, and thus an observation of differences between

pp and $p\bar{p}$ would be a clear signal of the odderon. Indeed, strong evidence for the odderon has been given in Ref. [77] based on a model-independent analysis of the combined TOTEM and D0 results in the dip-bump region.

B. Our standard results for the $pp \rightarrow pp\gamma$ reaction and comparison with soft-photon approximations

First, we present our exact model or standard bremsstrahlung results for the $pp \rightarrow pp\gamma$ reaction (see Sec. II C) for the proton-proton collision energy $\sqrt{s} = 13$ TeV. Below, k_\perp is the absolute value of the photon transverse momentum, $\omega = k^0$ is the center-of-mass photon energy, and y is the rapidity of the photon. Then, we will compare the resulting distributions with those obtained via variants of the SPA discussed in Sec. III.

We see from Fig. 4 that at $\sqrt{s} = 13$ TeV the pp -scattering cross section is completely dominated by the Pomeron exchange. Therefore, in the following, we shall take into account only the Pomeron-exchange contribution as shown in the diagrams of Figs. 3(a)–3(f).

In Fig. 7, we show the distributions in $|t_{1,2}|$, where $t_{1,2}$ is either t_1 or t_2 defined in (2.28), and in transverse momentum of the proton (here, $p_{t,p} = |\mathbf{p}'_{t,1}|$ or $|\mathbf{p}'_{t,2}|$). At $t_{1,2} = 0$ and $p_{t,p} = 0$, all contributions vanish. We can see how the $t_{1,2}$ distributions are sensitive to the form factor in the $\mathbb{P}pp$ vertex (A11) and $\epsilon_{\mathbb{P}}$ the Pomeron intercept parameter; see the discussion after Eq. (A2). In the following, we take in our calculations $\epsilon_{\mathbb{P}} = 0.0865$ and the exponential Pomeron-proton form factor $F(t) = \exp(-b|t|)$ with $b = 2.95 \text{ GeV}^{-2}$ adjusted to the TOTEM data (see Fig. 5). We see from Fig. 7 that photons with $1 \text{ MeV} < k_\perp < 100 \text{ MeV}$ and $|y| < 5$ come predominantly from pp collisions with momentum transfers between the protons of order $p_{t,p} \sim \sqrt{|t_{1,2}|} \sim 0.3 \text{ GeV}$. Very small values of $p_{t,p}$ and/or $|t_{1,2}|$ hardly contribute.

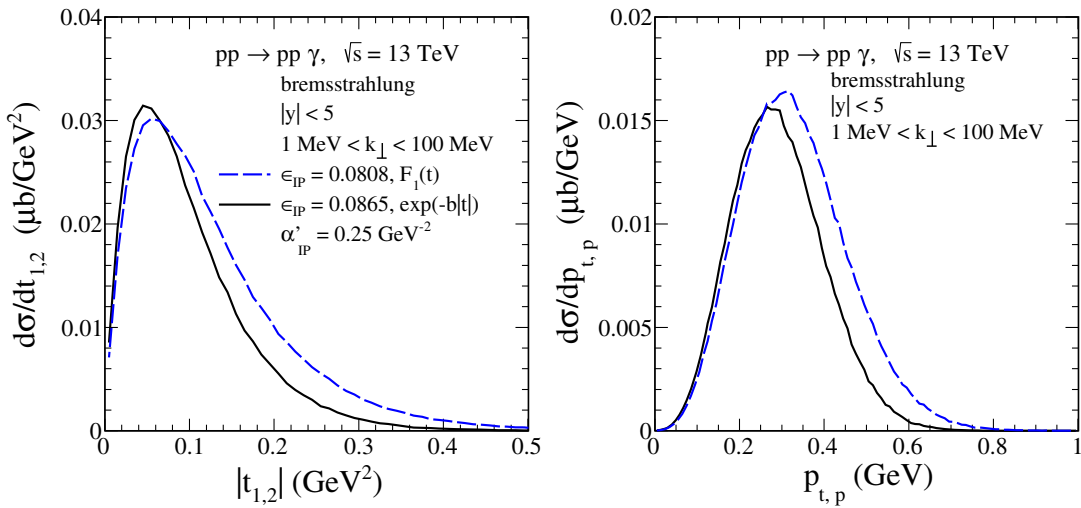


FIG. 7. The distributions in 4-momentum transfer squared $|t_{1,2}|$ and in the transverse momentum of the outgoing protons for the $pp \rightarrow pp\gamma$ reaction calculated for $\sqrt{s} = 13$ TeV, $|y| < 5$, and $1 \text{ MeV} < k_\perp < 100 \text{ MeV}$. The meaning of the lines is the same as in Fig. 5.

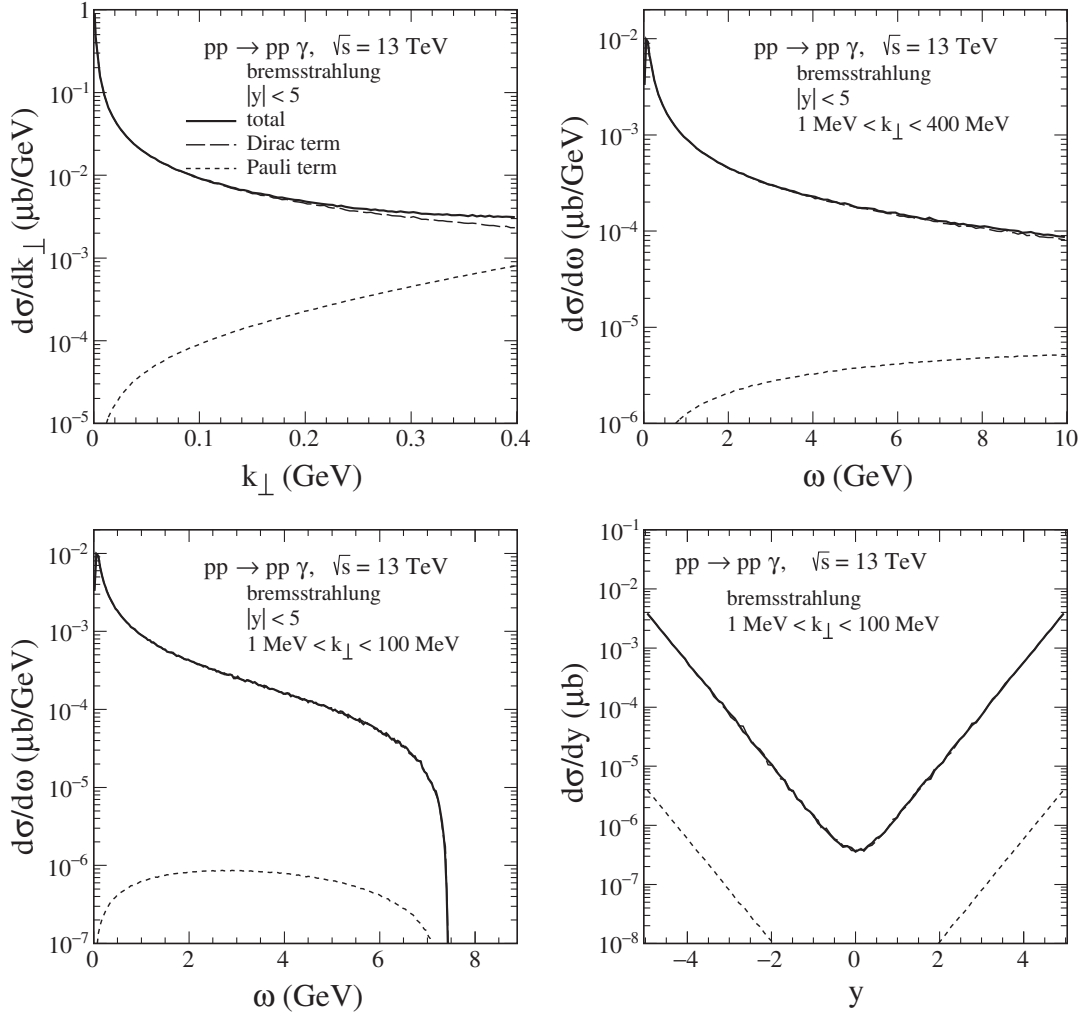


FIG. 8. The differential cross sections for the $pp \rightarrow pp\gamma$ reaction calculated for $\sqrt{s} = 13$ TeV, $|y| < 5$, and for the k_{\perp} intervals as specified in the figure legends. Shown are our standard results (total) and the results for the Dirac and Pauli terms alone.

In Fig. 8, we show the results obtained for $\sqrt{s} = 13$ TeV, $|y| < 5$, and for two k_{\perp} intervals: $1 \text{ MeV} < k_{\perp} < 400 \text{ MeV}$ (top panels) and $1 \text{ MeV} < k_{\perp} < 100 \text{ MeV}$ (bottom panels). We see that in the small k_{\perp} and ω regions the Dirac term from the γpp vertex function (2.37) dominates, while for larger values, the anomalous magnetic moment of the proton (Pauli term) plays an important role. Of course, for the complete result, all contributions to $\mathcal{M}_{\mu}^{(\text{standard})}$ from the diagrams of Fig. 3 with Dirac and Pauli terms have to be added coherently. For more details on the size of various contributions to $\mathcal{M}_{\mu}^{(\text{standard})}$, we refer to the discussions in Appendix B. We get the integrated cross sections for $\sqrt{s} = 13$ TeV and in the k_{\perp} range $1 \text{ MeV} < k_{\perp} < 100 \text{ MeV}$: $\sigma(pp \rightarrow pp\gamma) = 0.21 \text{ nb}$ for $|y| < 3.5$ and $\sigma(pp \rightarrow pp\gamma) = 4.01 \text{ nb}$ for $3.5 < |y| < 5$.

In Fig. 9 (left panels), we show the two-dimensional differential cross sections in the ω - k_{\perp} plane calculated for $\sqrt{s} = 13$ TeV, $1 \text{ MeV} < k_{\perp} < 100 \text{ MeV}$, $|y| < 3.5$ (the top panel) and $3.5 < |y| < 5$ (the bottom panel). The latter

rapidity range is relevant for the planned ALICE 3 measurements [16–18] of ultrasoft photons. Large y is near the ω axis, and $y = 0$ corresponds to the line $\omega = k_{\perp}$, both in accordance with $\omega = k_{\perp} \cosh y$. The phase-space region where $\omega < k_{\perp}$ is forbidden. We see that, due to our cuts on y and k_{\perp} applied in phase space, there are additional regions that are not accessible kinematically.

In the right panels of Fig. 9, we show the ratio

$$R(\omega, k_{\perp}) = \frac{d^2\sigma_{\text{SPA2}}/d\omega dk_{\perp}}{d^2\sigma_{\text{standard}}/d\omega dk_{\perp}}. \quad (4.2)$$

One can see that the SPA2 given by (3.4) stays within 1% accuracy for $k_{\perp} \lesssim 22 \text{ MeV}$ and $\omega \lesssim 0.35 \text{ GeV}$ considering $|y| < 3.5$ and up to $\omega \cong 1.7 \text{ GeV}$ for $3.5 < |y| < 5.0$. It is difficult to draw the ratio $R(\omega, k_{\perp})$ for SPA1/standard due to different integration procedures in two different codes: one for the exact three-body phase space (standard approach) and one for the two-body phase space supplemented by additional integration over photon 3-momentum (SPA1).

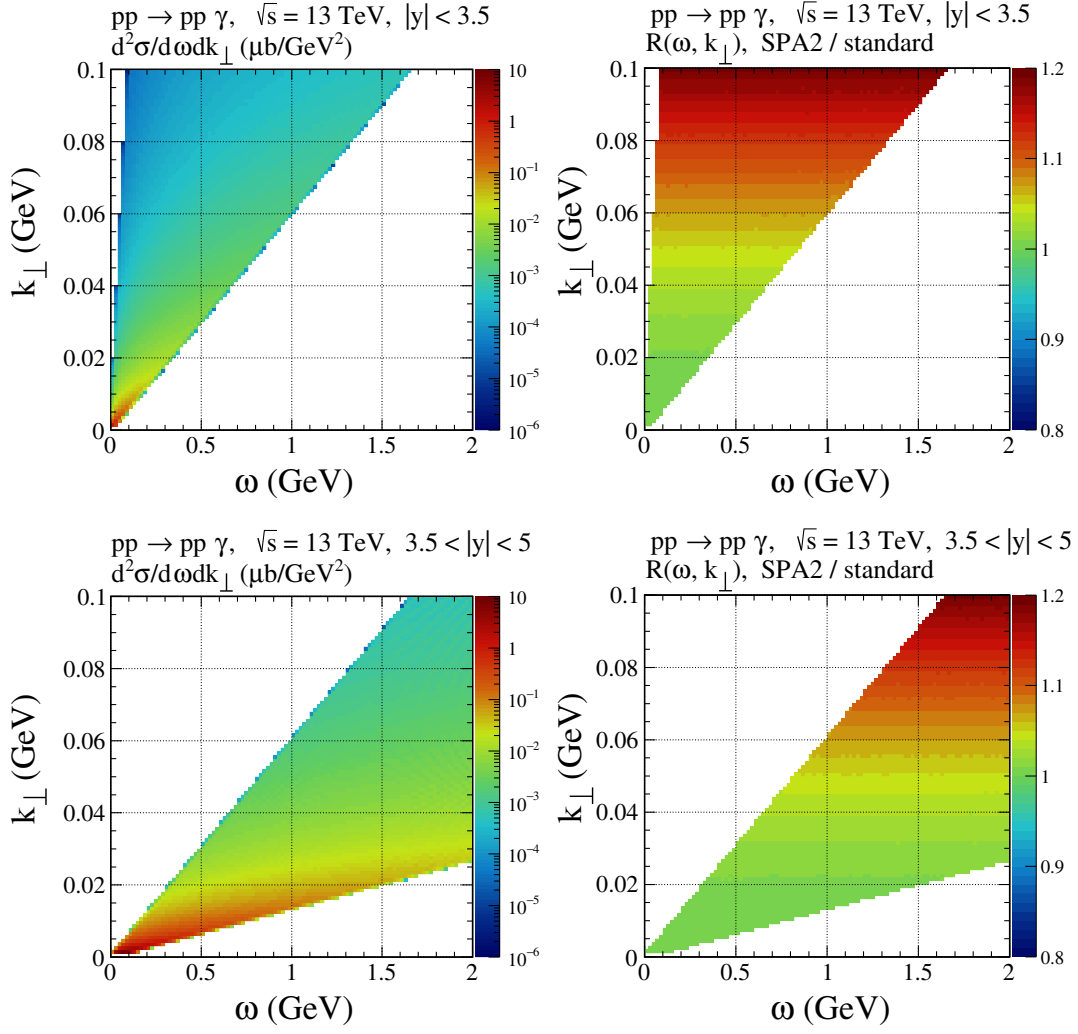


FIG. 9. The left panels show the cross section $d^2\sigma/d\omega dk_\perp$ as a function of (ω, k_\perp) calculated for $\sqrt{s} = 13$ TeV. The top panels are for $1 \text{ MeV} < k_\perp < 100 \text{ MeV}$, $|y| < 3.5$, and the bottom panels are for $3.5 < |y| < 5$. The right panels show the ratio $R(\omega, k_\perp)$ as defined in (4.2).

In Fig. 10, we compare our standard result to various SPAs on a semilogarithmic scale. We see that both, the SPA1 (3.1) and SPA2 (3.4), follow the standard results very well. Surprisingly, the SPA1, which does not have the correct energy-momentum relations, fares somewhat better than SPA2. But let us now have a closer look at these kinematic regions on a linear scale.

Figure 11 shows the ratios of the SPAs to the standard cross sections,

$$\frac{d\sigma_{\text{SPA}}/dk_\perp}{d\sigma_{\text{standard}}/dk_\perp}, \quad (4.3)$$

$$\frac{d\sigma_{\text{SPA}}/d\omega}{d\sigma_{\text{standard}}/d\omega}, \quad (4.4)$$

as functions of k_\perp and ω , respectively. The fluctuations of the ratio SPA1/standard (see the red dashed lines) are due to

a different organization of integration in the two codes. One can see that the deviations of the SPA1 from the standard results are up to around 1% for $|y| < 3.5$, $1 \text{ MeV} < k_\perp < 100 \text{ MeV}$, and $\omega \lesssim 0.7 \text{ GeV}$. For the forward region, $3.5 < |y| < 5$, this accuracy occurs even up to larger $\omega \simeq 2 \text{ GeV}$. For the SPA2, the deviations increase rapidly with growing k_\perp and ω (see also the right panels of Fig. 9).

In Fig. 12, we show the results for the SPA1 (3.5) and SPA2 (3.6) Ansätze using the high-energy small-angle approximation. The calculations were done for $\sqrt{s} = 13 \text{ TeV}$, $1 \text{ MeV} < k_\perp < 400 \text{ MeV}$, and $|y| < 5$. From the left panel, we see that the SPA1 is in very good agreement with our standard result if we include there only the Dirac terms. We have checked numerically that the results from (3.1) and (3.5) overlap. From the right panel, we see that the SPA2 results (3.4) and (3.6) are very close to each other.

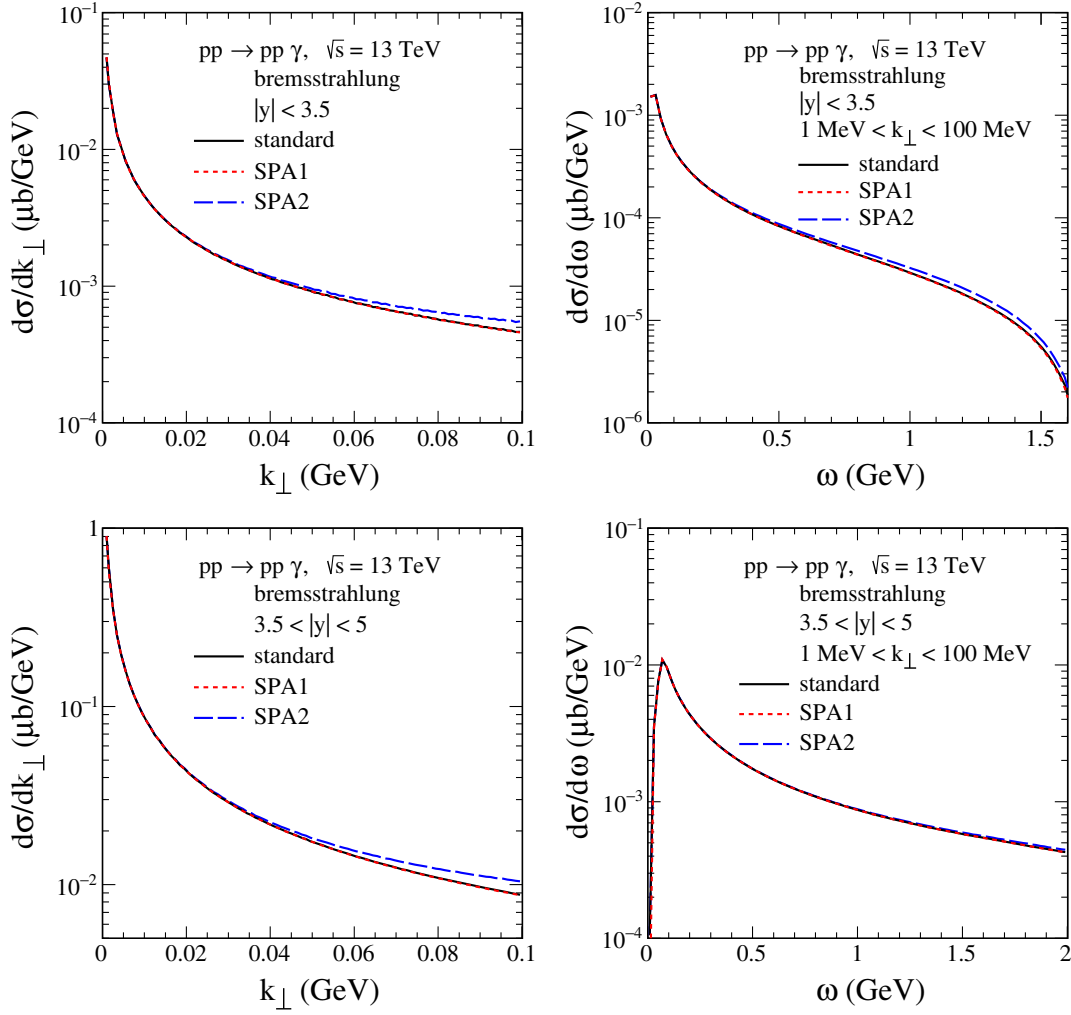


FIG. 10. The differential distributions in transverse momentum of the photon and in the energy of the photon for the $pp \rightarrow pp\gamma$ reaction. The calculations were done for $\sqrt{s} = 13$ TeV, $1 \text{ MeV} < k_{\perp} < 100 \text{ MeV}$, $|y| < 3.5$ (the top panels) and $3.5 < |y| < 5$ (the bottom panels). The black solid line corresponds to the standard result (2.62), the red dotted line corresponds to SPA1 (3.1), and the blue long-dashed line corresponds to SPA2 (3.4).

C. Comments on the photon radiation in connection with diffractive excitation of the proton

One may ask about the role of diffractive excitations of the protons in connection with photon radiation. There are two types of exclusive processes to be considered,

$$p + p \rightarrow p + \gamma + N^*, \quad (4.5)$$

with the N^* charged nucleon resonance decaying hadronically, typically $N^* \rightarrow p\pi^0$, $p\pi^0\pi^0$, $p\pi^+\pi^-$, and

$$p + p \rightarrow (N^* \rightarrow p + \gamma) + p, \quad (4.6)$$

$$p + p \rightarrow (N^* \rightarrow p + \gamma) + (N^* \rightarrow \text{hadrons}). \quad (4.7)$$

Relevant examples of diagrams for these processes with Pomeron exchange are shown in Fig. 13 for the reaction (4.5) and in Fig. 14 for (4.6) and (4.7).

The reactions (4.5) and (4.7) lead to a final state $p + \gamma + p + \text{pion}(s)$. Thus, there is no interference with the process $pp \rightarrow pp\gamma$ which we study in this paper. Of course, the question of whether experimentally the processes (4.5) and (4.7) can be separated from the elastic process (2.3) is a very relevant one. However, this will depend on the experiment and must be studied by the experimentalists themselves. The reaction (4.6), on the other hand, leads to the final state $pp\gamma$ and, thus, should be discussed here. Let us first note that the diagram of Fig. 14(a) will *not* lead in the amplitude to a bremsstrahlung term $\propto \omega^{-1}$. Indeed, this diagram will lead in the amplitude to a factor, for real photons where $k^2 = 0$,

$$\begin{aligned} & [(p'_1 + k)^2 - m_{N^*}^2 + im_{N^*}\Gamma_{N^*}]^{-1} \\ & = [2(p'_1 \cdot k) - (m_{N^*}^2 - m_p^2) + im_{N^*}\Gamma_{N^*}]^{-1}. \end{aligned} \quad (4.8)$$

Here, m_{N^*} and Γ_{N^*} are the mass and width of the N^* resonance considered. Clearly, Eq. (4.8) will *not* lead to a singular

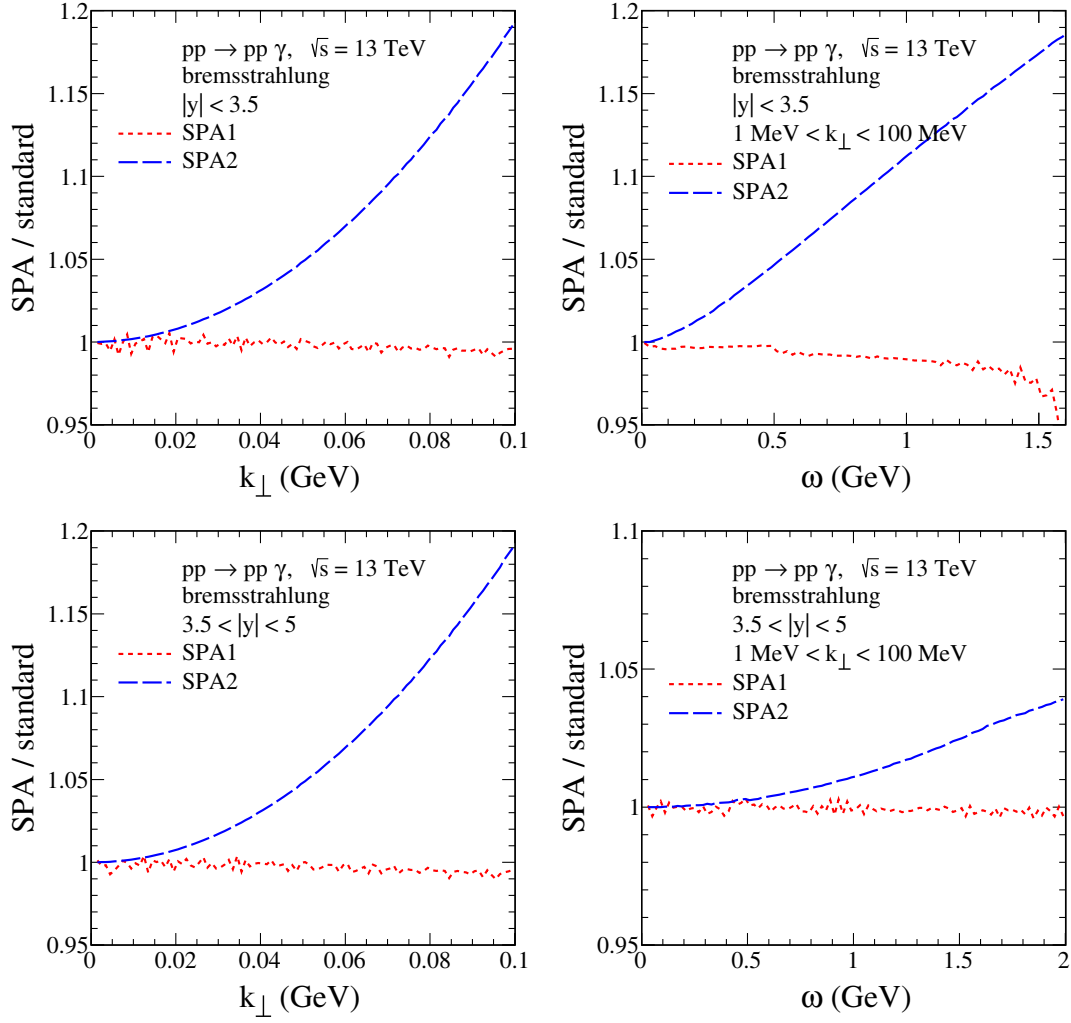


FIG. 11. The ratios $\sigma_{\text{SPA}}/\sigma_{\text{standard}}$ given by (4.3) and (4.4), respectively. The red dotted line corresponds to SPA1 (3.1), and the blue long-dashed line corresponds to SPA2 (3.4). The oscillations in the SPA1 results are of numerical origin.

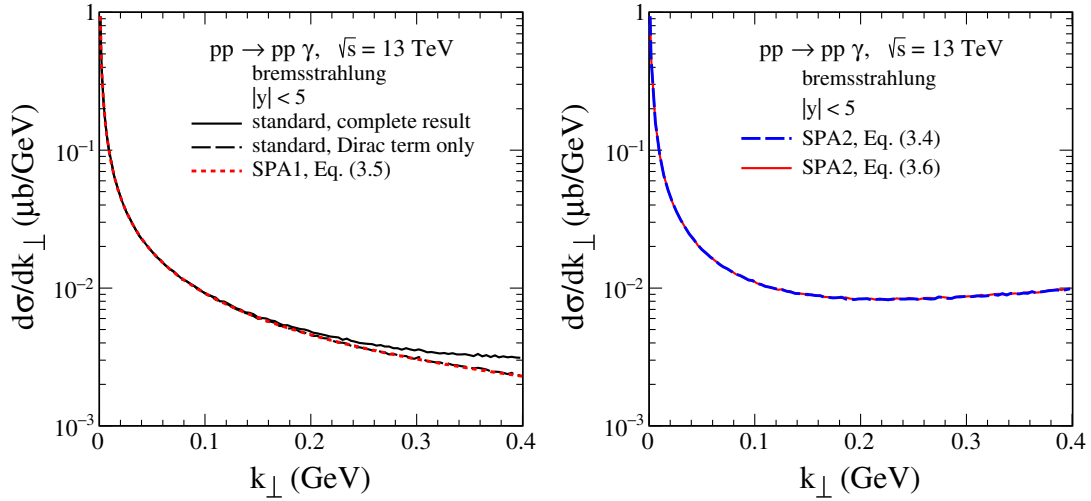


FIG. 12. Comparison of the cross sections $d\sigma/dk_{\perp}$ for our standard bremsstrahlung model and the SPA1 (left panel) and for the two versions of the SPA2 (right panel). In the left panel, we show the standard complete result and the result for the Dirac term alone from Fig. 8 together with the SPA1 result (3.5). In the right panel, the blue long-dashed line corresponds to (3.4), while the red solid line corresponds to (3.6).

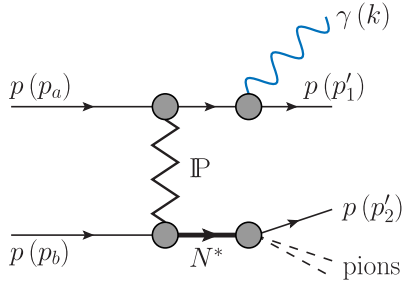


FIG. 13. A diagram for the reaction (4.5) with photon emission from the proton line and hadronic decay of the N^* . The diagrams where the photon is attached in all other possible ways to the charged particle lines are not shown.

contribution as $k \rightarrow 0$. Thus, in our terminology, it is part of the structure term (g) of Fig. 3. In the following, we give a short discussion of N^* resonances which can contribute to the photon flux via the diagrams of the type of Fig. 14(a).

The $N(1440)$ with $J^P = 1/2^+$, $N(1520)$ with $J^P = 3/2^-$, and $N(1680)$ with $J^P = 5/2^+$ states are potential candidates for the role of N^* in (4.6). These resonances satisfy the Gribov-Morrison rule; see, e.g., Chap. 3.9 of Ref. [46]. The Roper resonance $N(1440)$ is doubtful. This poorly known state was considered, however, in Refs. [56,78] as an important contribution to forward low-mass single

diffraction dissociation. In Ref. [33], it was shown for the $pp \rightarrow pp\pi^0$ reaction that the nonresonant diffractive processes (Drell-Hiida-Deck type model) lead to an enhancement in the invariant mass $M_{\pi p} \approx 1.4$ GeV. Thus, one cannot be sure whether the Roper resonance plays an important role there. Coming back to the $pp \rightarrow (N^* \rightarrow p\gamma)p$ reaction, the Roper resonance has much smaller branching ratio [65] $\mathcal{BR}(N(1440) \rightarrow p\gamma) = 0.035\text{--}0.048\%$ than the $N(1520)$, $\mathcal{BR}(N(1520) \rightarrow p\gamma) = 0.31\text{--}0.52\%$, and the $N(1680)$, $\mathcal{BR}(N(1680) \rightarrow p\gamma) = 0.21\text{--}0.32\%$. For the $N(1680)$ resonance, a sizeable cross section $\sigma(pp \rightarrow pN(1680)) = 170 \pm 60 \mu\text{b}$ was estimated at the CERN ISR energy of $\sqrt{s} = 45$ GeV [79]. One should, however, bear in mind that at ISR energies secondary reggeon exchanges are still important. For the bremsstrahlung-type processes at the LHC energies, the reggeon-exchange contributions are very small; thus, diffractively excited N^* resonances are there due to Pomeron exchange and should be produced preferentially in forward/backward rapidity region. All these processes require dedicated studies if the low γp invariant-mass region can be measured in the forward rapidity range.

In Fig. 15, we show the differential cross sections $d\sigma/dM_{\gamma p, \text{low}}$ (the same sign rapidity of γ and p) and $d\sigma/dM_{\gamma p, \text{high}}$ (the opposite sign rapidity of γ and p) for our standard bremsstrahlung (nonresonant) model. The

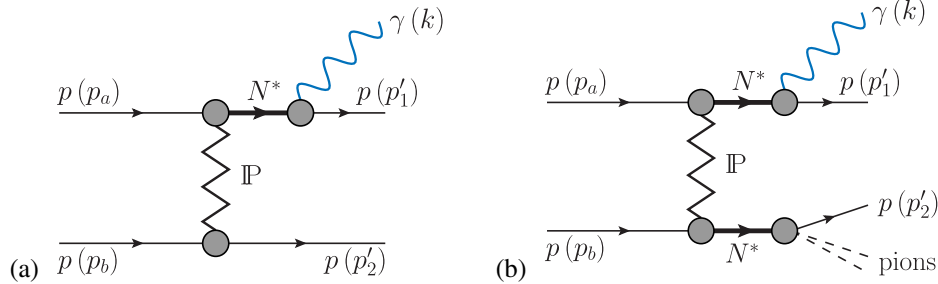


FIG. 14. Examples of diagrams: (a) for the reaction (4.6) and (b) for the reaction (4.7).

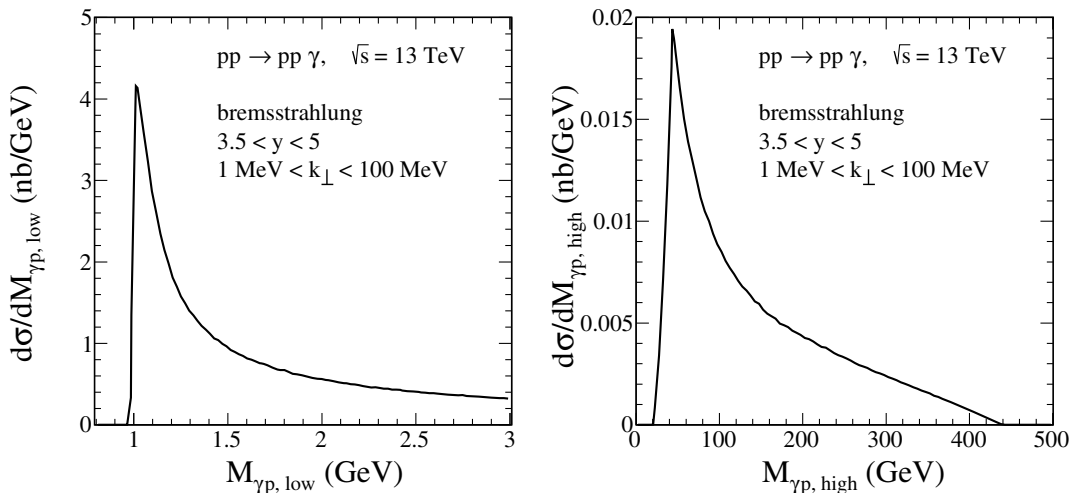


FIG. 15. The distributions in $M_{\gamma p, \text{low}}$ (left panel) and in $M_{\gamma p, \text{high}}$ (right panel) for our standard bremsstrahlung (nonresonant) model.

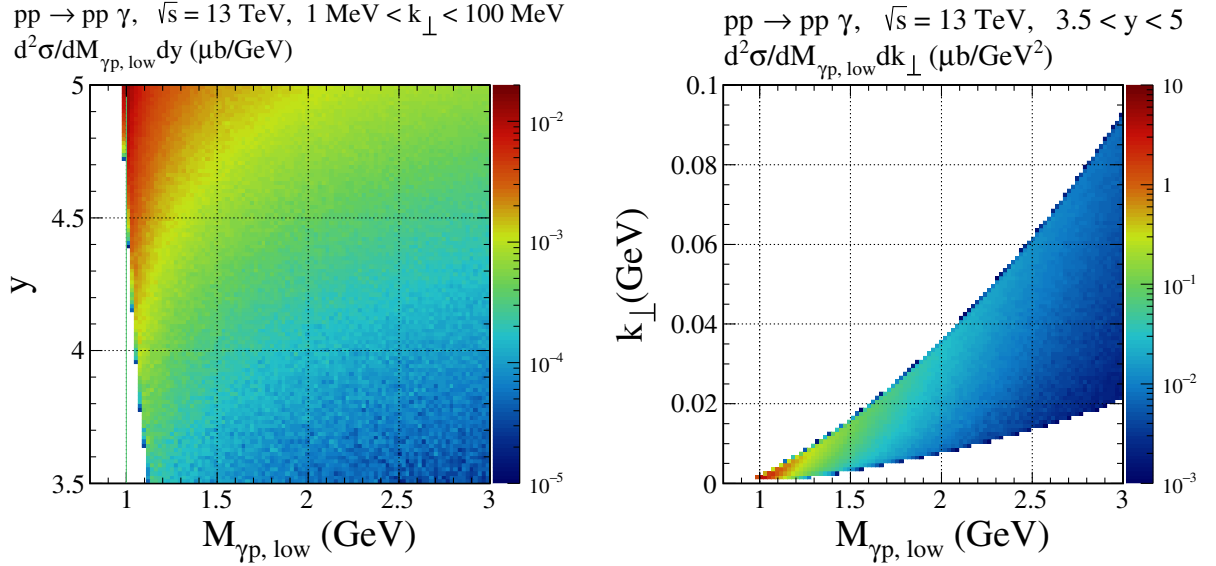


FIG. 16. The two-dimensional distributions in $(M_{\gamma p, \text{low}}, y)$ and in $(M_{\gamma p, \text{low}}, k_{\perp})$ for the $pp \rightarrow pp\gamma$ reaction for our standard bremsstrahlung (nonresonant) model.

calculations were done for $\sqrt{s} = 13 \text{ TeV}$, $3.5 < y < 5$, and $1 \text{ MeV} < k_{\perp} < 100 \text{ MeV}$. Figure 16 shows the two-dimensional distributions in $(M_{\gamma p, \text{low}}, y)$ and in $(M_{\gamma p, \text{low}}, k_{\perp})$. In the present paper, we consider soft-photon emission only by protons. As already mentioned, photons may also be produced from the radiative decays of diffractively excited nucleon resonances. Candidates are $N(1440)$, $N(1520)$, and $N(1680)$. If these processes contribute significantly to our $pp \rightarrow pp\gamma$ reaction, then we should see them in the $M_{\gamma p, \text{low}}$ distribution (possibly distorted by interference effects) as a resonance enhancement at $M_{\gamma p} = m_{N^*}$ with a width Γ_{N^*} over our nonresonant term. However, we expect that the decay photons will be emitted at rapidities larger than covered by the dedicated ALICE 3 detector. Other background contributions, for instance, soft photons from central-exclusive production via the fusion processes $\gamma\mathbb{P} \rightarrow \gamma$, $\mathbb{O}\mathbb{P} \rightarrow \gamma$, etc., should be taken into account. Possible interference effects between various mechanisms should be also included. This goes beyond the scope of the present paper. We leave a detailed analysis of other contributions for future studies. Finally, we conclude that the measurement of forward/backward protons would be crucial for a better understanding of the mechanisms of the $pp \rightarrow pp\gamma$ reaction.

V. CONCLUSIONS

In this paper, we have presented a detailed discussion of the reactions $pp \rightarrow pp$, $p\bar{p} \rightarrow p\bar{p}$, and $pp \rightarrow pp\gamma$ at high c.m. energies using the framework of the tensor-Pomeron model [28]. To calculate the amplitudes for these reactions, we have considered Pomeron (\mathbb{P}), odderon (\mathbb{O}), and reggeon ($f_{2\mathbb{R}}$, $a_{2\mathbb{R}}$, $\omega_{\mathbb{R}}$, $\rho_{\mathbb{R}}$) exchanges.

Our theoretical results for elastic pp and $p\bar{p}$ scattering are given in Secs. II A and II B and compared to experimental

data in Secs. IV A and IV B. With our model, adjusting the Pomeron and odderon parameters, we get a reasonable fit to the TOTEM data on pp elastic scattering for $\sqrt{s} = 13 \text{ TeV}$ and $|t| \lesssim 0.3 \text{ GeV}^2$; see Fig. 5. We emphasize that we are not out to produce a precision fit to all pp and $p\bar{p}$ elastic scattering data. We only need a reasonable description of the data for $\sqrt{s} = 13 \text{ TeV}$ as a prerequisite for the calculation of photon radiation in pp collisions at this energy. Nevertheless, we also had a look at the data for ρ , the ratio of real and imaginary parts of the forward-scattering amplitudes. We found that, taking the TOTEM data for granted, we need an odderon contribution in the framework of our model, and a double Regge pole structure of this odderon with intercept slightly above 1 seems to be preferred; see Fig. 6. Clearly, further experimental studies of reactions where odderon effects could be present would be very welcome. Examples of such reactions are photoproduction of f_2 mesons, $\gamma p \rightarrow f_2 p$, and central exclusive production of single and double ϕ mesons, $pp \rightarrow p\phi p$ and $pp \rightarrow p\phi\phi p$; see, for instance, Refs. [80–82]. All these reactions can be studied at ALICE3.

Turning now to the main topic of our paper, the calculation of soft-photon radiation in pp collisions, we have given the explicit formulas for this process in the framework of our tensor-Pomeron model. The amplitudes corresponding to photon emission from the external proton lines [see the diagrams of Figs. 3(a), 3(b), 3(d), and 3(e)] are determined by the off-shell $pp \rightarrow pp$ scattering amplitude. By construction, the amplitudes (c) and (f), the contact terms, have to satisfy gauge-invariance constraints involving the previous amplitudes. In this way, we obtained our standard results for the $pp \rightarrow pp\gamma$ reaction. The relevant distributions are shown in Figs. 7–11.

We have compared our standard results to two soft-photon approximations SPA1 and SPA2; see Sec. III. In

the SPA1, we considered only the pole terms $\propto \omega^{-1}$ in the radiative amplitudes. This SPA1 agrees rather well, at the percent level, with our exact model (or standard result) in the kinematic range considered; see Figs. 10 and 11. For $1 \text{ MeV} < k_{\perp} < 100 \text{ MeV}$ and $3.5 < |y| < 5.0$, for

instance, we find agreement of SPA1 with our standard result at the percent level up to $\omega \cong 2 \text{ GeV}$. The SPA2 is a good approximation to the standard result, within 1% accuracy, for $k_{\perp} \lesssim 22 \text{ MeV}$ and $\omega \lesssim 0.35 \text{ GeV}$ considering $|y| < 3.5$ and up to $\omega \cong 1.7 \text{ GeV}$ for $3.5 < |y| < 5.0$; see Fig. 9.

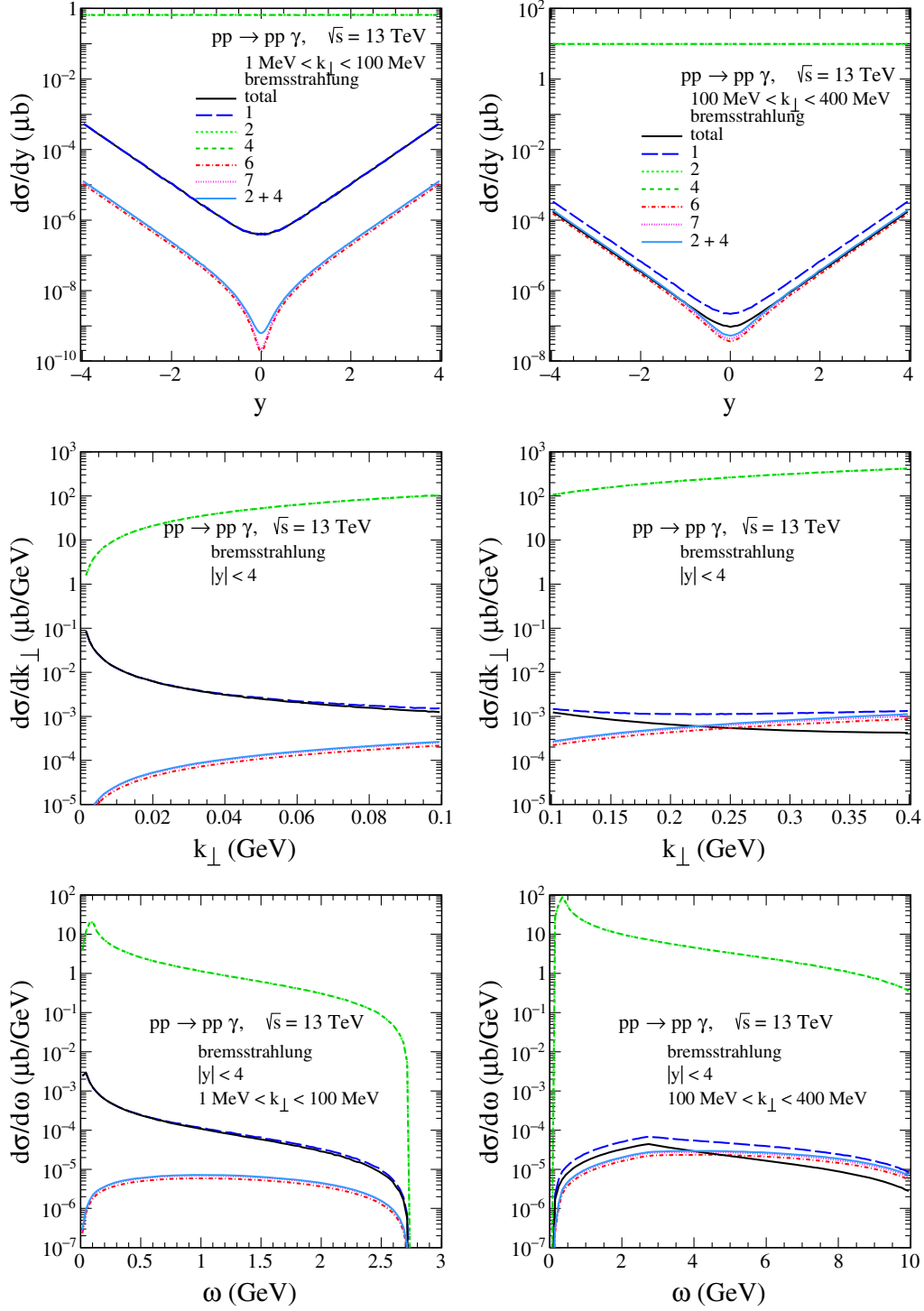


FIG. 17. The differential distributions for the $pp \rightarrow pp\gamma$ reaction calculated for $\sqrt{s} = 13 \text{ TeV}$, $|y| < 4$, and for two k_{\perp} intervals as specified in the figure legends. The results for individual j terms in (B3) and their coherent sum (total) are shown. The coherent sum of the amplitudes $(a + b + c)$ plus $(d + e + f)$ with $j = 2$ and $j = 4$ is denoted by “2 + 4”.

In Sec. II C, we have written the amplitude for $pp \rightarrow pp\gamma$ in the standard, straightforward, way with the photon coupling to the protons via the Dirac and Pauli terms. It turned out that the corresponding formulas (2.39), (2.40), (2.56), and (2.59)–(2.61) were not convenient for numerical work. Therefore, we have rewritten these amplitudes in Appendix B as a sum of seven terms, labeled by $j = 1, \dots, 7$, for the tensor exchanges and of four terms, labeled by $j' = 1, \dots, 4$, for the vector exchanges [see (B3)–(B16)]. Each of these 11 terms is separately gauge invariant. The pole terms are only contained in the $j = 1$ tensor term and $j' = 1$ vector term. The other terms have no singularity for $\omega \rightarrow 0$. Thus, one expects that for soft-photon emission the terms with $j = 1$ and $j' = 1$ will be dominant. We found that indeed this is correct but there is a very interesting effect guaranteeing this. Considering for Pomeron exchange the gauge-invariant and nonsingular terms with $j = 2$ and $j = 4$ alone, we find that the pole term only dominates over these $j = 2$ and $j = 4$ terms individually for very small $k_{\perp} \approx \omega \lesssim 2m_p^2/\sqrt{s} \cong 0.15$ MeV [see (B20), (B21), and Fig. 18]. This effect is, in essence, due to the Pauli coupling of the photon. We note that in the literature such small values for ω as a limit for the dominance of the ω^{-1} term are mentioned. For instance, in Ref. [23], it is argued that for hard high-energy elastic processes Low's original result gives a reliable representation of the radiative amplitude only in the vanishingly small region $\omega \lesssim m^2/Q$ in the limit $Q \rightarrow \infty$. Here, Q is the scale of the hard process, and m is the charged particle mass. But since in this work only *hard* processes with photon emission are considered, these arguments do not apply to our case. We consider the exclusive *soft* process $pp \rightarrow pp\gamma$ with soft-photon emission. We have, of course, to take *all* contributions with different labels j into account and add them coherently; see (B3). We find then large cancellations between the $j = 2$ and $j = 4$ terms; see Fig. 17. This leads to a much larger region in k_{\perp} and ω where the pole terms alone give a good representation of the radiative amplitude; see Fig. 9. Our conclusion is that simple order of magnitude estimates for the ω regions where the pole term dominates, using only parts of the amplitudes, may give completely wrong results. It is essential to add coherently all the various parts of the amplitude for soft-photon emission in order not to miss important interference effects.

In this article, we have only discussed the bremsstrahlung-type emission of soft photons in pp collisions. Anomalous emission terms have been subsumed in the amplitude $\mathcal{M}_{\mu}^{(g)}$,

which must satisfy (2.58) and can have no singularity for $k \rightarrow 0$. There are, however, quite conventional contributions to $\mathcal{M}_{\mu}^{(g)}$, for instance, soft photons from central-exclusive production via the fusion processes $\gamma^{\mathbb{P}} \rightarrow \gamma$, $\mathbb{O}^{\mathbb{P}} \rightarrow \gamma$. The contributions of such processes are expected to be important in the midrapidity region, around $y = 0$. In a future paper, we plan to study central-exclusive production of photons within the tensor-Pomeron approach.

Finally, we emphasize that we have taken care to write the formulas for the $pp \rightarrow pp\gamma$ amplitude in such a way that they also apply to soft virtual photon production, for instance, $pp \rightarrow pp(\gamma^* \rightarrow e^+e^-)$. Thus, our Eqs. (2.39), (2.40), (2.56), and (2.59)–(2.61), as well as (B1)–(B16), can be directly used for soft virtual photon production. But further investigations of this interesting topic go beyond the scope of our present article.

We hope that our theoretical studies of the exclusive $pp \rightarrow pp\gamma$ reaction will find experimental counterparts with measurements of soft photons at the Relativistic Heavy Ion Collider and at the LHC, for instance, with the planned ALICE3 detector [16–18].

ACKNOWLEDGMENTS

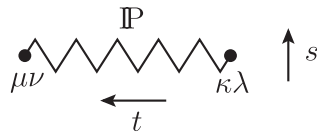
We thank Johanna Stachel, Peter Braun-Munzinger, and Carlo Ewerz for very useful discussions. We are grateful to Carlo Ewerz for reading the manuscript. This work and the stay of Piotr Lebedowicz in Heidelberg were supported by the Bekker Program of the Polish National Agency for Academic Exchange under Contract No. BPN/BEK/2021/2/00009/U/00001. This study was also partially supported by the Polish National Science Centre under Grant No. 2018/31/B/ST2/03537.

APPENDIX A: LIST OF QUANTITIES AND THEIR VALUES USED IN THE PAPER

The quantities listed in the following are in essence taken from Chap. 3 of Ref. [28]. Here, the propagators and vertices involving the Pomeron, the odderon, and the reggeons are to be understood as effective propagators and vertices.

The effective propagators for \mathbb{P} , reggeons, and \mathbb{O} are as follows:

- (i) Pomeron \mathbb{P} (see (3.10), (3.11), and Sec. 6.1 of Ref. [28]):

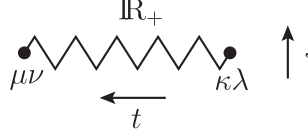


$$i\Delta_{\mu\nu,\kappa\lambda}^{(\mathbb{P})}(s, t) = \frac{1}{4s} \left(g_{\mu\kappa}g_{\nu\lambda} + g_{\mu\lambda}g_{\nu\kappa} - \frac{1}{2}g_{\mu\nu}g_{\kappa\lambda} \right) (-isa'_{\mathbb{P}})^{\alpha_{\mathbb{P}}(t)-1}, \quad (\text{A1})$$

$$\begin{aligned}\alpha_{\mathbb{P}}(t) &= \alpha_{\mathbb{P}}(0) + \alpha'_{\mathbb{P}} t, & \alpha_{\mathbb{P}}(0) &= 1 + \epsilon_{\mathbb{P}}, \\ \alpha'_{\mathbb{P}} &= 0.25 \text{ GeV}^{-2}.\end{aligned}\quad (\text{A2})$$

The default value for $\epsilon_{\mathbb{P}}$ from Ref. [28] is $\epsilon_{\mathbb{P}} = 0.0808$. In our present paper, we find from a comparison to the data from TOTEM measurements at $\sqrt{s} = 13 \text{ TeV}$ [64,67] a slightly higher value: $\epsilon_{\mathbb{P}} = 0.0865$; see Fig. 5. This value for the soft Pomeron intercept is in agreement with those obtained in Refs. [83–85]. Our value above also agrees, within practically 1 standard deviation, with that obtained in Ref. [42] from a fit to photoproduction and low- x deep inelastic scattering which gave $\epsilon_{\mathbb{P}} = 0.0935^{+76}_{-64}$.

(ii) reggeons $\mathbb{R}_+ = f_{2\mathbb{R}}, a_{2\mathbb{R}}$ (see (3.12), (3.13), and Sec. 6.3 of Ref. [28]):



$$i\Delta_{\mu\nu,\kappa\lambda}^{(\mathbb{R}_+)}(s, t) = \frac{1}{4s} \left(g_{\mu\kappa} g_{\nu\lambda} + g_{\mu\lambda} g_{\nu\kappa} - \frac{1}{2} g_{\mu\nu} g_{\kappa\lambda} \right) (-is\alpha'_{\mathbb{R}_+})^{\alpha_{\mathbb{R}_+}(t)-1}, \quad (\text{A3})$$

$$\begin{aligned}\alpha_{\mathbb{R}_+}(t) &= \alpha_{\mathbb{R}_+}(0) + \alpha'_{\mathbb{R}_+} t, \\ \alpha_{\mathbb{R}_+}(0) &= 0.5475, \\ \alpha'_{\mathbb{R}_+} &= 0.9 \text{ GeV}^{-2}.\end{aligned}\quad (\text{A4})$$

(iii) reggeons $\mathbb{R}_- = \omega_{\mathbb{R}}, \rho_{\mathbb{R}}$ (see (3.14), (3.15), and Sec. 6.3 of Ref. [28]):

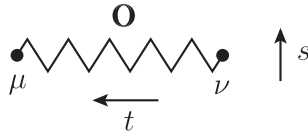


$$i\Delta_{\mu\nu}^{(\mathbb{R}_-)}(s, t) = ig_{\mu\nu} \frac{1}{M_-^2} (-is\alpha'_{\mathbb{R}_-})^{\alpha_{\mathbb{R}_-}(t)-1}, \quad (\text{A5})$$

$$\begin{aligned}\alpha_{\mathbb{R}_-}(t) &= \alpha_{\mathbb{R}_-}(0) + \alpha'_{\mathbb{R}_-} t, \\ \alpha_{\mathbb{R}_-}(0) &= 0.5475, \\ \alpha'_{\mathbb{R}_-} &= 0.9 \text{ GeV}^{-2}, \\ M_- &= 1.41 \text{ GeV}.\end{aligned}\quad (\text{A6})$$

The numbers for the reggeon parameters in (A4) and (A6) are taken from Ref. [47] and Figs. 3.1 and 3.2 of Ref. [46], except for M_- , which is discussed in Sec. 6.3 of Ref. [28].

(iv) odderon \mathbb{O} :



Our Ansatz for a single-pole odderon is as in Ref. [28] [see (3.16), (3.17), and Sec. 6.2 therein]:

$$i\Delta_{\mu\nu}^{(\mathbb{O})}(s, t) = -ig_{\mu\nu} \frac{\eta_{\mathbb{O}}}{M_0^2} (-is\alpha'_{\mathbb{O}})^{\alpha_{\mathbb{O}}(t)-1}, \quad (\text{A7})$$

$$\begin{aligned}\alpha_{\mathbb{O}}(t) &= \alpha_{\mathbb{O}}(0) + \alpha'_{\mathbb{O}} t, & \alpha_{\mathbb{O}}(0) &= 1 + \epsilon_{\mathbb{O}}, \\ M_0 &= 1 \text{ GeV}, \\ \eta_{\mathbb{O}} &= \pm 1, \\ \alpha'_{\mathbb{O}} &= 0.25 \text{ GeV}^{-2}.\end{aligned}\quad (\text{A8})$$

Here, $M_0 = 1 \text{ GeV}$ is introduced for dimensional reasons, and $\alpha'_{\mathbb{O}} = \alpha'_{\mathbb{P}}$ (A2) is set as default.

For a double-pole odderon, we set

$$i\tilde{\Delta}_{\mu\nu}^{(\mathbb{O})}(s, t) = i\Delta_{\mu\nu}^{(\mathbb{O})}(s, t)[C_1 + C_2 \ln(-is\alpha'_{\mathbb{O}})]. \quad (\text{A9})$$

Here, C_1 and C_2 are real constants.

From the comparison with the ρ values of pp and $p\bar{p}$ scattering, we find that the following values give a reasonable description of the TOTEM data (see Fig. 6):

$$\begin{aligned}\eta_{\mathbb{O}} &= -1, & \alpha'_{\mathbb{O}} &= 0.25 \text{ GeV}^{-2}, & \epsilon_{\mathbb{O}} &= 0.0800, \\ (C_1, C_2) &= (-1.0, 0.1), (-1.5, 0.2), (-2.0, 0.3).\end{aligned}\quad (\text{A10})$$

The effective proton-Pomeron, proton-reggeon, and proton-odderon vertices are taken as in Ref. [28], but at least for the $\mathbb{P}pp$ vertex, we use a different form factor in order to fit the TOTEM data [64,67] at $\sqrt{s} = 13$ TeV and in the low $|t|$ region. Now here is the list of effective vertices.

(i) $\mathbb{P}pp$ vertex (see (3.43), (3.44), and Sec. 6.1 of Ref. [28]):

$$(A11)$$

$$\begin{aligned} i\Gamma_{\mu\nu}^{(\mathbb{P}pp)}(p', p) &= i\Gamma_{\mu\nu}^{(\mathbb{P}\bar{p}\bar{p})}(p', p) \\ &= -i3\beta_{\mathbb{P}pp}F_1[(p' - p)^2] \\ &\quad \times \left\{ \frac{1}{2} \left[\gamma_\mu(p' + p)_\nu + \gamma_\nu(p' + p)_\mu \right] - \frac{1}{4}g_{\mu\nu}(\not{p}' + \not{p}) \right\}, \end{aligned}$$

$$\beta_{\mathbb{P}pp} = 1.87 \text{ GeV}^{-1}. \quad (A12)$$

In Ref. [28], the form factor $F_1(t)$ was taken as the electromagnetic form factor of the proton,

$$\begin{aligned} F_1(t) &= \left(1 - \frac{t}{4m_p^2} \frac{\mu_p}{\mu_N}\right) \left(1 - \frac{t}{4m_p^2}\right)^{-1} G_D(t), \\ \mu_N &= \frac{e}{2m_p}, \quad \frac{\mu_p}{\mu_N} = 2.7928, \\ G_D(t) &= \left(1 - \frac{t}{m_D^2}\right)^{-2}, \quad m_D^2 = 0.71 \text{ GeV}^2. \end{aligned} \quad (A13)$$

In the present paper, we use $F_1(t) \rightarrow F(t) = \exp(-b|t|)$ with $b = 2.95 \text{ GeV}^{-2}$ adjusted to the TOTEM data (see Fig. 5).

(ii) \mathbb{R}_+pp vertex, where $\mathbb{R}_+ = f_{2\mathbb{R}}, a_{2\mathbb{R}}$ (see (3.49)–(3.52) and Sec. 6.3 of Ref. [28]):

$$(A14)$$

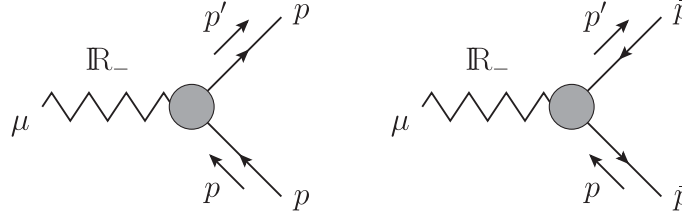
$$\begin{aligned} i\Gamma_{\mu\nu}^{(f_{2\mathbb{R}}pp)}(p', p) &= i\Gamma_{\mu\nu}^{(f_{2\mathbb{R}}\bar{p}\bar{p})}(p', p) \\ &= -ig_{f_{2\mathbb{R}}pp} \frac{1}{M_0} F_1[(p' - p)^2] \\ &\quad \times \left\{ \frac{1}{2} \left[\gamma_\mu(p' + p)_\nu + \gamma_\nu(p' + p)_\mu \right] - \frac{1}{4}g_{\mu\nu}(\not{p}' + \not{p}) \right\}, \end{aligned}$$

$$g_{f_{2\mathbb{R}}pp} = 11.04, \quad M_0 = 1 \text{ GeV}; \quad (A15)$$

$$\begin{aligned}
i\Gamma_{\mu\nu}^{(a_{2R}pp)}(p', p) &= i\Gamma_{\mu\nu}^{(a_{2R}\bar{p}\bar{p})}(p', p) \\
&= -ig_{a_{2R}pp} \frac{1}{M_0} F_1[(p' - p)^2] \left\{ \frac{1}{2} [\gamma_\mu(p' + p)_\nu + \gamma_\nu(p' + p)_\mu] - \frac{1}{4} g_{\mu\nu}(\not{p}' + \not{p}) \right\}, \quad (\text{A16})
\end{aligned}$$

$$g_{a_{2R}pp} = 1.68, \quad M_0 = 1 \text{ GeV}. \quad (\text{A17})$$

(iii) \mathbb{R}_-pp vertex, where $\mathbb{R}_- = \omega_{\mathbb{R}}, \rho_{\mathbb{R}}$ (see (3.59)–(3.62) and Sec. 6.3 of Ref. [28]):



$$(\text{A18})$$

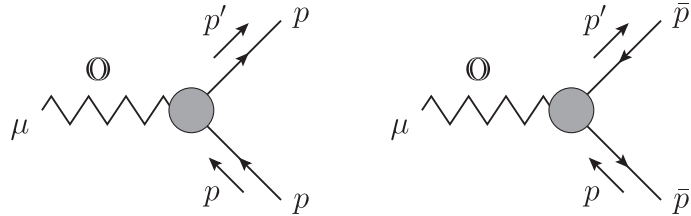
$$\begin{aligned}
i\Gamma_{\mu}^{(\omega_{\mathbb{R}}pp)}(p', p) &= -i\Gamma_{\mu}^{(\omega_{\mathbb{R}}\bar{p}\bar{p})}(p', p) \\
&= -ig_{\omega_{\mathbb{R}}pp} F_1[(p' - p)^2] \gamma_{\mu},
\end{aligned}$$

$$g_{\omega_{\mathbb{R}}pp} = 8.65; \quad (\text{A19})$$

$$\begin{aligned}
i\Gamma_{\mu}^{(\rho_{\mathbb{R}}pp)}(p', p) &= -i\Gamma_{\mu}^{(\rho_{\mathbb{R}}\bar{p}\bar{p})}(p', p) \\
&= -ig_{\rho_{\mathbb{R}}pp} F_1[(p' - p)^2] \gamma_{\mu}, \quad (\text{A20})
\end{aligned}$$

$$g_{\rho_{\mathbb{R}}pp} = 2.02. \quad (\text{A21})$$

(iv) $\mathbb{O}pp$ vertex (see (3.68), (3.69), and Sec. 6.2 of Ref. [28]):



$$(\text{A22})$$

$$\begin{aligned}
i\Gamma_{\mu}^{(\mathbb{O}pp)}(p', p) &= -i\Gamma_{\mu}^{(\mathbb{O}\bar{p}\bar{p})}(p', p) \\
&= -i3\beta_{\mathbb{O}pp} M_0 F_1[(p' - p)^2] \gamma_{\mu},
\end{aligned}$$

$$\beta_{\mathbb{O}pp} = 0.2 \text{ GeV}^{-1}, \quad M_0 = 1 \text{ GeV}. \quad (\text{A23})$$

The coupling constant $\beta_{\mathbb{O}pp}$ is taken as free parameter to be determined by experiment. In the present study, we assume (A23): $\beta_{\mathbb{O}pp} = 0.1 \times \beta_{\mathbb{P}pp} \simeq 0.2 \text{ GeV}^{-1}$.

At the end of this Appendix, we give the formulas corresponding to (2.49), (2.50), and (2.54) for the case of a double-pole odderon (A9). We have here to replace $\mathcal{F}_{\mathbb{O}pp}(s, t)$ by $\tilde{\mathcal{F}}_{\mathbb{O}pp}(s, t)$ according to (2.17). In this way, we get instead of (2.49)

$$\tilde{\mathcal{F}}_{\mathbb{O}pp}(s', t_2) = \tilde{\mathcal{F}}_{\mathbb{O}pp}(s, t_2) + \varkappa \widetilde{\Delta \mathcal{F}}_{\mathbb{O}pp}(s, t_2, \varkappa), \quad (\text{A24})$$

where

$$\widetilde{\Delta\mathcal{F}}_{\mathbb{O}pp}(s, t_2, \boldsymbol{x}) = \mathcal{F}_{\mathbb{O}pp}(s, t_2) \left\{ C_1(1 - \alpha_{\mathbb{O}}(t_2))g_{\mathbb{O}}(\boldsymbol{x}, t_2) + C_2 \left[(1 - \alpha_{\mathbb{O}}(t_2))g_{\mathbb{O}}(\boldsymbol{x}, t_2) \ln(-is(1 - \boldsymbol{x})\alpha'_{\mathbb{O}}) + \frac{1}{\boldsymbol{x}} \ln(1 - \boldsymbol{x}) \right] \right\}. \quad (\text{A25})$$

For $\Delta\mathcal{F}_V(s, t, \boldsymbol{x})$ in (2.54), this gives the replacement

$$\widetilde{\Delta\mathcal{F}}_V(s, t, \boldsymbol{x}) = \widetilde{\Delta\mathcal{F}}_{\mathbb{O}pp}(s, t, \boldsymbol{x}) + (1 - \alpha_{\omega_{\mathbb{R}}}(t))g_{\omega_{\mathbb{R}}}(\boldsymbol{x}, t)\mathcal{F}_{\omega_{\mathbb{R}}pp}(s, t) + (1 - \alpha_{\rho_{\mathbb{R}}}(t))g_{\rho_{\mathbb{R}}}(\boldsymbol{x}, t)\mathcal{F}_{\rho_{\mathbb{R}}pp}(s, t). \quad (\text{A26})$$

APPENDIX B: THE AMPLITUDES WITH PHOTON EMISSION

Here, we rewrite the amplitude $\mathcal{M}_{\mu}^{(a+b+c)} = \mathcal{M}_{\mu}^{(a)} + \mathcal{M}_{\mu}^{(b)} + \mathcal{M}_{\mu}^{(c)}$, see (2.39), (2.40), and (2.56), in a way that is more suitable for numerical computations.

We use the following relations:

$$\begin{aligned} \frac{\not{p}_a - \not{k} + m_p}{(p_a - k)^2 - m_p^2 + i\epsilon} \left(\gamma_{\mu} - \frac{i}{2m_p} \sigma_{\mu\nu} k^{\nu} F_2(0) \right) u_a &= \frac{1}{-2p_a \cdot k + k^2 + i\epsilon} \left\{ 2p_{a\mu} - k_{\mu} + (k_{\mu} - \not{k}\gamma_{\mu}) \right. \\ &\quad \left. + \frac{F_2(0)}{2m_p} \left[2(p_{a\mu}\not{k} - (p_a \cdot k)\gamma_{\mu}) + 2m_p(k_{\mu} - \not{k}\gamma_{\mu}) - (\not{k}k_{\mu} - k^2\gamma_{\mu}) \right] \right\} u_a, \end{aligned} \quad (\text{B1})$$

$$\begin{aligned} \bar{u}_{1'} \left(\gamma_{\mu} - \frac{i}{2m_p} \sigma_{\mu\nu} k^{\nu} F_2(0) \right) \frac{\not{p}'_1 + \not{k} + m_p}{(p'_1 + k)^2 - m_p^2 + i\epsilon} &= \bar{u}_{1'} \frac{1}{2p'_1 \cdot k + k^2 + i\epsilon} \left\{ 2p'_{1\mu} + k_{\mu} - (k_{\mu} - \gamma_{\mu}\not{k}) \right. \\ &\quad \left. + \frac{F_2(0)}{2m_p} \left[-2(p'_{1\mu}\not{k} - (p'_1 \cdot k)\gamma_{\mu}) - 2m_p(k_{\mu} - \gamma_{\mu}\not{k}) - (k_{\mu}\not{k} - k^2\gamma_{\mu}) \right] \right\}. \end{aligned} \quad (\text{B2})$$

Using (B1) and (B2) and exploiting the properties of the Dirac spinors, $\not{p}_a u_a = m_p u_a$, $\bar{u}_{1'} \not{p}'_1 = \bar{u}_{1'} m_p$ etc., we can write our $\mathcal{M}_{\mu}^{(\text{standard})}$ from (2.62) as follows:

$$\mathcal{M}_{\mu}^{(\text{standard})} = \sum_{j=1}^7 (\mathcal{M}_{\text{T},\mu}^{(a+b+c)j} + \mathcal{M}_{\text{T},\mu}^{(d+e+f)j}) + \sum_{j'=1}^4 (\mathcal{M}_{\text{V},\mu}^{(a+b+c)j'} + \mathcal{M}_{\text{V},\mu}^{(d+e+f)j'}). \quad (\text{B3})$$

Here, T and V stand for the tensor- and vector-exchange diagrams, respectively, and j and j' are just labels for the subamplitudes in the sums on the rhs of (B3). We have

$$\begin{aligned} \mathcal{M}_{\text{T},\mu}^{(a+b+c)1} &= e\bar{u}_{1'} \otimes \bar{u}_{2'} \left\{ i\mathcal{F}_T(s, t_2) [\gamma^{\alpha} \otimes \gamma_{\alpha}(p_a + p'_1, p_b + p'_2) + (\not{p}_b + \not{p}'_2) \otimes (\not{p}_a + \not{p}'_1)] \right. \\ &\quad \left. - 2m_p^2 \mathbb{1} \otimes \mathbb{1} \left[\frac{2p_{a\mu} - k_{\mu}}{-2p_a \cdot k + k^2 + i\epsilon} + \frac{2p'_{1\mu} + k_{\mu}}{2p'_1 \cdot k + k^2 + i\epsilon} \right] \right\} u_a \otimes u_b, \end{aligned} \quad (\text{B4})$$

$$\begin{aligned} \mathcal{M}_{\text{T},\mu}^{(a+b+c)2} &= e\bar{u}_{1'} \otimes \bar{u}_{2'} \left\{ i\mathcal{F}_T(s', t_2) \frac{1}{-2p_a \cdot k + k^2 + i\epsilon} [\gamma^{\alpha} \otimes \gamma_{\alpha}(p_a + p'_1 - k, p_b + p'_2)] \right. \\ &\quad + (\not{p}_b + \not{p}'_2) \otimes (\not{p}_a + \not{p}'_1 - \not{k}) \left[k_{\mu} - \not{k}\gamma_{\mu} + \frac{F_2(0)}{2m_p} (2p_{a\mu}\not{k} - 2(p_a \cdot k)\gamma_{\mu}) \right. \\ &\quad \left. \left. + 2m_p(k_{\mu} - \not{k}\gamma_{\mu}) - (\not{k}k_{\mu} - k^2\gamma_{\mu}) \right] \otimes \mathbb{1} \right\} u_a \otimes u_b, \end{aligned} \quad (\text{B5})$$

$$\begin{aligned}
\mathcal{M}_{T,\mu}^{(a+b+c)3} = & -e\bar{u}_{1'} \otimes \bar{u}_{2'} \left\{ i\mathcal{F}_T(s', t_2) \frac{m_p}{-2p_a \cdot k + k^2 + i\epsilon} \left[2p_{a\mu}\not{k} - 2(p_a \cdot k)\gamma_\mu + 2m_p(k_\mu - \not{k}\gamma_\mu) \right. \right. \\
& - (\not{k}k_\mu - k^2\gamma_\mu) + \frac{F_2(0)}{2m_p} ((-2(p_a \cdot k) + k^2 + 4m_p^2)(k_\mu - \not{k}\gamma_\mu) \\
& \left. \left. + 2m_p(2p_{a\mu}\not{k} - 2(p_a \cdot k)\gamma_\mu) - 2m_p(\not{k}k_\mu - k^2\gamma_\mu) \right] \otimes \mathbb{1} \right\} u_a \otimes u_b, \tag{B6}
\end{aligned}$$

$$\begin{aligned}
\mathcal{M}_{T,\mu}^{(a+b+c)4} = & e\bar{u}_{1'} \otimes \bar{u}_{2'} \left\{ i\mathcal{F}_T(s, t_2) \frac{1}{2p'_1 \cdot k + k^2 + i\epsilon} \left[-(k_\mu - \gamma_\mu\not{k}) \right. \right. \\
& \left. \left. + \frac{F_2(0)}{2m_p} (-2p'_{1\mu}\not{k} + 2(p'_1 \cdot k)\gamma_\mu - 2m_p(k_\mu - \gamma_\mu\not{k}) - (k_\mu\not{k} - k^2\gamma_\mu)) \right] \otimes \mathbb{1} \right. \\
& \left. \times [\gamma^\alpha \otimes \gamma_\alpha(p_a + p'_1 + k, p_b + p'_2) + (\not{p}_b + \not{p}'_2) \otimes (\not{p}_a + \not{p}'_1 + \not{k})] \right\} u_a \otimes u_b, \tag{B7}
\end{aligned}$$

$$\begin{aligned}
\mathcal{M}_{T,\mu}^{(a+b+c)5} = & -e\bar{u}_{1'} \otimes \bar{u}_{2'} \left\{ i\mathcal{F}_T(s, t_2) \frac{m_p}{2p'_1 \cdot k + k^2 + i\epsilon} \left[-2p'_{1\mu}\not{k} + 2(p'_1 \cdot k)\gamma_\mu - 2m_p(k_\mu - \gamma_\mu\not{k}) \right. \right. \\
& - (\not{k}k_\mu - k^2\gamma_\mu) - \frac{F_2(0)}{2m_p} ((2(p'_1 \cdot k) + k^2 + 4m_p^2)(k_\mu - \gamma_\mu\not{k}) \\
& \left. \left. + 2m_p(2p'_{1\mu}\not{k} - 2(p'_1 \cdot k)\gamma_\mu) + 2m_p(\not{k}k_\mu - k^2\gamma_\mu) \right] \otimes \mathbb{1} \right\} u_a \otimes u_b, \tag{B8}
\end{aligned}$$

$$\begin{aligned}
\mathcal{M}_{T,\mu}^{(a+b+c)6} = & e\bar{u}_{1'} \otimes \bar{u}_{2'} \left\{ i\Delta\mathcal{F}_T(s, t_2, \boldsymbol{x}) [\gamma^\alpha \otimes \gamma_\alpha(p_a + p'_1 - k, p_b + p'_2) \right. \\
& \left. + (\not{p}_b + \not{p}'_2) \otimes (\not{p}_a + \not{p}'_1 - \not{k}) - m_p(2m_p - \not{k}) \otimes \mathbb{1} \right] \\
& \left. \times \left[\frac{(2p_a + 2p_b - k, k)}{s} \frac{2p_{a\mu} - k_\mu}{-2p_a \cdot k + k^2 + i\epsilon} + \frac{(2p_a + 2p_b - k)_\mu}{s} \right] \right\} u_a \otimes u_b, \tag{B9}
\end{aligned}$$

$$\begin{aligned}
\mathcal{M}_{T,\mu}^{(a+b+c)7} = & e\bar{u}_{1'} \otimes \bar{u}_{2'} \left\{ i\mathcal{F}_T(s, t_2) \left[(\gamma^\alpha \otimes \gamma_\alpha(p_b + p'_2, k) + (\not{p}_b + \not{p}'_2) \otimes \not{k} - m_p\not{k} \otimes \mathbb{1}) \right. \right. \\
& \left. \left. \times \left(\frac{2p'_{1\mu} + k_\mu}{2p'_1 \cdot k + k^2 + i\epsilon} - \frac{2p_{a\mu} - k_\mu}{-2p_a \cdot k + k^2 + i\epsilon} \right) \right. \right. \\
& \left. \left. - 2\gamma^\alpha \otimes \gamma_\alpha(p_b + p'_2)_\mu - 2(\not{p}_b + \not{p}'_2) \otimes \gamma_\mu + 2m_p\gamma_\mu \otimes \mathbb{1} \right] \right\} u_a \otimes u_b. \tag{B10}
\end{aligned}$$

For the subamplitudes with the vector exchanges, we get

$$\mathcal{M}_{V,\mu}^{(a+b+c)1} = -e\bar{u}_{1'} \otimes \bar{u}_{2'} \left\{ \mathcal{F}_V(s, t_2) \gamma^\alpha \otimes \gamma_\alpha \left[\frac{2p_{a\mu} - k_\mu}{-2p_a \cdot k + k^2 + i\epsilon} + \frac{2p'_{1\mu} + k_\mu}{2p'_1 \cdot k + k^2 + i\epsilon} \right] \right\} u_a \otimes u_b, \tag{B11}$$

$$\mathcal{M}_{V,\mu}^{(a+b+c)2} = -e\bar{u}_{1'} \otimes \bar{u}_{2'} \left\{ \Delta\mathcal{F}_V(s, t_2, \boldsymbol{x}) \gamma^\alpha \otimes \gamma_\alpha \left[\frac{(2p_a + 2p_b - k, k)}{s} \frac{2p_{a\mu} - k_\mu}{-2p_a \cdot k + k^2 + i\epsilon} + \frac{(2p_a + 2p_b - k)_\mu}{s} \right] \right\} u_a \otimes u_b, \tag{B12}$$

$$\begin{aligned}
\mathcal{M}_{V,\mu}^{(a+b+c)3} = & -e\bar{u}_{1'} \otimes \bar{u}_{2'} \left\{ \mathcal{F}_V(s', t_2) \frac{1}{-2p_a \cdot k + k^2 + i\epsilon} \gamma^\alpha \left[k_\mu - \not{k}\gamma_\mu + \frac{F_2(0)}{2m_p} (2p_{a\mu}\not{k} - 2(p_a \cdot k)\gamma_\mu + 2m_p(k_\mu - \not{k}\gamma_\mu) \right. \right. \\
& \left. \left. - (\not{k}k_\mu - k^2\gamma_\mu) \right] \otimes \gamma_\alpha \right\} u_a \otimes u_b, \tag{B13}
\end{aligned}$$

$$\begin{aligned} \mathcal{M}_{\sqrt{\mu}}^{(a+b+c)4} = & -e\bar{u}_{1'} \otimes \bar{u}_{2'} \left\{ \mathcal{F}_V(s, t_2) \frac{1}{2p'_1 \cdot k + k^2 + i\epsilon} \left[-(k_\mu - \gamma_\mu \not{k}) \right. \right. \\ & \left. \left. + \frac{F_2(0)}{2m_p} (-2p'_{1\mu} \not{k} + 2(p'_1 \cdot k)\gamma_\mu - 2m_p(k_\mu - \gamma_\mu \not{k}) - (k_\mu \not{k} - k^2 \gamma_\mu)) \right] \gamma^\alpha \otimes \gamma_\alpha \right\} u_a \otimes u_b. \end{aligned} \quad (\text{B14})$$

According to (2.59)–(2.61), we have

$$\mathcal{M}_{T,\mu}^{(d+e+f)j} = \mathcal{M}_{T,\mu}^{(a+b+c)j} \Big|_{\substack{(p_a, \lambda_a) \leftrightarrow (p_b, \lambda_b) \\ (p'_1, \lambda_1) \leftrightarrow (p'_2, \lambda_2)}} \quad \text{for } j = 1, \dots, 7, \quad (\text{B15})$$

$$\mathcal{M}_{V,\mu}^{(d+e+f)j'} = \mathcal{M}_{V,\mu}^{(a+b+c)j'} \Big|_{\substack{(p_a, \lambda_a) \leftrightarrow (p_b, \lambda_b) \\ (p'_1, \lambda_1) \leftrightarrow (p'_2, \lambda_2)}} \quad \text{for } j' = 1, \dots, 4, \quad (\text{B16})$$

where we also exchange the order of the tensor products in (B4)–(B14). Note that all subamplitudes $\mathcal{M}_{T,\mu}^{(a+b+c)j}$ and $\mathcal{M}_{V,\mu}^{(a+b+c)j'}$ are separately gauge invariant, as is easy to check,

$$\begin{aligned} k^\mu \mathcal{M}_{T,\mu}^{(a+b+c)j} &= 0, \quad j = 1, \dots, 7, \\ k^\mu \mathcal{M}_{V,\mu}^{(a+b+c)j'} &= 0, \quad j' = 1, \dots, 4. \end{aligned} \quad (\text{B17})$$

The same holds for $\mathcal{M}_{T,\mu}^{(d+e+f)j}$ and $\mathcal{M}_{V,\mu}^{(d+e+f)j'}$.

Note that only the $j = 1$ terms in (B4) and (B15) and the $j' = 1$ terms in (B11) and (B16) contain the pole terms proportional to ω^{-1} for $\omega \rightarrow 0$. The SPA1 and SPA2 results are derived from these terms; see Sec. III.

In Fig. 17, we show differential distributions for the $pp \rightarrow pp\gamma$ reaction for $\sqrt{s} = 13$ TeV, $|y| < 4$, and for two k_\perp intervals: $1 \text{ MeV} < k_\perp < 100 \text{ MeV}$ (the left panels), $100 \text{ MeV} < k_\perp < 400 \text{ MeV}$ (the right panels). In these calculations, we limit ourselves to the leading Pomeron-exchange contribution. We show the complete result (“total”) including interference effects and the results for individual j terms (B4)–(B10) plus (B15), except for $j = 3$ and 5, which are very small and can be safely neglected. Note that there is significant cancellation among the terms $j = 2$ and 4, due to destructive interference. The coherent sum of the amplitudes $(a + b + c)$ plus $(d + e + f)$ with $j = 2$ and $j = 4$ is denoted by $2 + 4$.

How can we understand these results? First, we remark that the destructive interference of the 2 and 4 terms above is *not* due to a gauge cancellation. These terms are separately gauge invariant; see (B17). Let us have a closer look at the terms 1, 2, and 4 of (B4), (B5), and (B7), respectively, for real photons, $k^2 = 0$, and with transverse momentum only:

$$(k^\mu) = \begin{pmatrix} \omega \\ \omega \hat{\mathbf{k}}_\perp \end{pmatrix}, \quad |\hat{\mathbf{k}}_\perp| = 1. \quad (\text{B18})$$

We work in the c.m. system with $|\mathbf{p}_a|$ defining the z axis. Then, disregarding terms on the rhs of (B4) and (B5), which are of the same order in $|\mathbf{p}_a|$, we get very roughly

$$\begin{aligned} \mathcal{M}_{T,\mu}^{(a+b+c)1} &\propto \frac{p_{a\mu}}{-p_a \cdot k} + \frac{p'_{1\mu}}{p'_1 \cdot k} \\ &\propto \frac{\Delta p}{|\mathbf{p}_a| \omega}. \end{aligned} \quad (\text{B19})$$

Here, $\Delta p = \mathcal{O}(m_p)$ is a measure of the transverse momentum change from \mathbf{p}_a to \mathbf{p}'_1 .

The term $\mathcal{M}_{T,\mu}^{(a+b+c)2}$ has no singularity for $\omega \rightarrow 0$. The main term here comes from the anomalous magnetic moment $F_2(0)$ and can be estimated as

$$\mathcal{M}_{T,\mu}^{(a+b+c)2} \propto \frac{1}{|\mathbf{p}_a| \omega} \frac{|\mathbf{p}_a| \omega}{m_p} = \frac{1}{m_p} \quad (\text{B20})$$

and similarly for $\mathcal{M}_{T,\mu}^{(a+b+c)4}$. Thus, the term $\mathcal{M}_{T,\mu}^{(a+b+c)1}$ will win over the 2 and 4 terms individually for $\omega \rightarrow 0$. However, for this to happen, we must require

$$\begin{aligned} \frac{\Delta p}{|\mathbf{p}_a| \omega} &\approx \frac{m_p}{|\mathbf{p}_a| \omega} \gtrsim \frac{1}{m_p}, \\ \omega &\lesssim \frac{m_p^2}{|\mathbf{p}_a|}. \end{aligned} \quad (\text{B21})$$

For our case with $2|\mathbf{p}_a| = 13$ TeV, this requires

$$k_\perp \approx \omega \lesssim 0.15 \text{ MeV}. \quad (\text{B22})$$

Explicit calculations confirm the order of magnitude of this estimate. Indeed, from Fig. 18, we see that the $j = 1$ term exceeds the $j = 2$ term only for $k_\perp \lesssim 0.35$ MeV and $\omega \lesssim 0.7$ MeV. The crossing place of these terms depends on the y range since the $j = 1$ term has a minimum at $y = 0$ and grows rapidly with $|y|$ increasing, while the terms 2 and 4 are flat in the midrapidity region (see the top panels of Fig. 17). When going with $y \rightarrow 0$, the crossing place of the terms 1 and 2 shifts to lower values of k_\perp and ω . In reality, however, there is destructive interference between the terms 2 and 4, and their *sum* is harmless, well below the term 1, at least for $k_\perp < 100$ MeV and $\omega < 2$ GeV, as we see from the left panels of Fig. 17. In the right panels of Fig. 17, we show the results for larger k_\perp and ω ranges. The destructive interference of the terms 2 and 4 is again a salient feature.

As we mentioned already, the terms with labels $j = 2$ and 4 contain the Dirac and Pauli couplings, and the latter

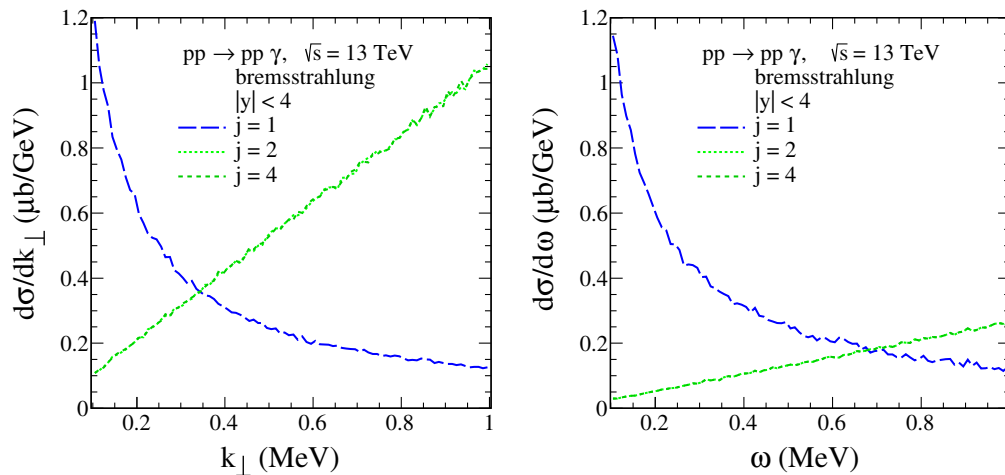


FIG. 18. The cross sections $d\sigma/dk_{\perp}$ (left) and $d\sigma/d\omega$ (right) for the terms $\mathcal{M}_{T,\mu}^{(a+b+c)j} + \mathcal{M}_{T,\mu}^{(d+e+f)j}$ for Pomeron exchange for $j = 1, 2,$ and 4 . See (B4), (B5), (B7), and (B15). The crossing of the term $j = 1$ containing the ω^{-1} pole with the nonpole terms $j = 2$ and 4 occurs for $k_{\perp} \cong 0.35$ MeV and $\omega \cong 0.7$ MeV.

one dominates. In the result $2 + 4$ shown in Fig. 17, we find destructive interference of the Pauli parts of $j = 2$ and $j = 4$ in the term $(a + b + c)$ and in the term $(d + e + f)$ individually. But for the Pauli parts, we find numerically that there is practically no interference between the $(a + b + c)$ and the $(d + e + f)$ terms. In the $2 + 4$ term, the Dirac part wins over the Pauli part. The visible dip for $d\sigma/dy$ at $y \approx 0$ in the $2 + 4$ result (see the left upper panel of Fig. 17) is due to destructive interference of the Dirac parts between the $(a + b + c)$ and the $(d + e + f)$ terms.

For the vector-exchange contributions, (B11)–(B14) and (B16), the situation is similar to that for the tensor exchanges. The terms containing the ω^{-1} pole are the $j' = 1$ terms. Individually, the vector-exchange terms with $j' = 3$ and $j' = 4$ are much larger than the $j' = 1$ term, except for very small k_{\perp} and ω . But again there is destructive interference of the $j' = 3$ and $j' = 4$ terms, and the sum $3 + 4$ is well below the $j' = 1$ term in the same kinematic regions as shown in Fig. 17. In this kinematic region, the $j' = 2$ term is very small.

-
- [1] P. Lebedowicz, O. Nachtmann, and A. Szczurek, High-energy $\pi\pi$ scattering without and with photon radiation, *Phys. Rev. D* **105**, 014022 (2022).
- [2] F. E. Low, Bremsstrahlung of very low-energy quanta in elementary particle collisions, *Phys. Rev.* **110**, 974 (1958).
- [3] A. T. Goshaw, J. R. Elliott, L. E. Evans, L. R. Fortney, P. W. Lucas, W. J. Robertson, W. D. Walker, I. J. Kim, and C.-R. Sun, Direct Photon Production from π^+p Interactions at 10.5 GeV/c, *Phys. Rev. Lett.* **43**, 1065 (1979).
- [4] P. V. Chliapnikov, E. A. De Wolf, A. B. Fenyuk, L. N. Gerdyukov, Y. Goldschmidt-Clermont, V. M. Ronzhin, and A. Weigend, (Brussels-CERN-Genoa-Mons-Nijmegen-Serpukhov Collaboration), Observation of direct soft photon production in K^+p interactions at 70 GeV/c, *Phys. Lett.* **141B**, 276 (1984).
- [5] F. Botterweck *et al.* (EHS/NA22 Collaboration), Direct soft photon production in K^+p and π^+p interactions at 250 GeV/c, *Z. Phys. C* **51**, 541 (1991).
- [6] S. Banerjee *et al.* (SOPHIE/WA83 Collaboration), Observation of direct soft photon production in π^-p interactions at 280 GeV/c, *Phys. Lett. B* **305**, 182 (1993).
- [7] J. Antos *et al.*, Soft photon production in 400 GeV/c p -Be collisions, *Z. Phys. C* **59**, 547 (1993).
- [8] M. L. Tincknell *et al.*, Low transverse momentum photon production in proton-nucleus collisions at 18 GeV/c, *Phys. Rev. C* **54**, 1918 (1996).
- [9] A. Belogianni *et al.* (WA91 Collaboration), Confirmation of a soft photon signal in excess of Q.E.D. expectations in π^-p interactions at 280 GeV/c, *Phys. Lett. B* **408**, 487 (1997).
- [10] A. Belogianni *et al.*, Further analysis of a direct soft photon excess in π^-p interactions at 280 GeV/c, *Phys. Lett. B* **548**, 122 (2002).
- [11] A. Belogianni *et al.*, Observation of a soft photon signal in excess of QED expectations in pp interactions, *Phys. Lett. B* **548**, 129 (2002).
- [12] J. Abdallah *et al.* (DELPHI Collaboration), Evidence for an excess of soft photons in hadronic decays of Z^0 , *Eur. Phys. J. C* **47**, 273 (2006).
- [13] J. Abdallah *et al.* (DELPHI Collaboration), Observation of the muon inner bremsstrahlung at LEP1, *Eur. Phys. J. C* **57**, 499 (2008).

- [14] J. Abdallah *et al.* (DELPHI Collaboration), Study of the dependence of direct soft photon production on the jet characteristics in hadronic Z^0 decays, *Eur. Phys. J. C* **67**, 343 (2010).
- [15] C.-Y. Wong, An overview of the anomalous soft photons in hadron production, Proc. Sci., Photon2013 (2014) 002 [arXiv:1404.0040].
- [16] D. Adamová *et al.*, A next-generation LHC heavy-ion experiment, arXiv:1902.01211.
- [17] P. Braun-Munzinger, Experimental opportunities for new physics at low transverse momentum, in *Proceedings of XXIXth International Conference on Ultra-relativistic Nucleus-Nucleus Collisions, Kraków, Poland, 2022*.
- [18] Workshop EMMI Rapid Reaction Task Force on “Real and virtual photon production at ultra-low transverse momentum and low mass at LHC”, organised by K. Schweda, R. Bailhache, and S. Flörchinger, <https://indico.gsi.de/event/11529/overview>.
- [19] V. N. Gribov, Bremsstrahlung of Hadrons at High Energies, *Sov. J. Nucl. Phys.* **5**, 280 (1967).
- [20] T. H. Burnett and N. M. Kroll, Extension of the Low Soft-Photon Theorem, *Phys. Rev. Lett.* **20**, 86 (1968).
- [21] J. S. Bell and R. Van Royen, On the low-Burnett-Kroll theorem for soft-photon emission, *Nuovo Cimento A* **60**, 62 (1969).
- [22] L. N. Lipatov, Massless particle bremsstrahlung theorems for high-energy hadron interactions, *Nucl. Phys.* **B307**, 705 (1988).
- [23] V. Del Duca, High-energy bremsstrahlung theorems for soft photons, *Nucl. Phys.* **B345**, 369 (1990).
- [24] H. Gervais, Soft photon theorem for high energy amplitudes in Yukawa and scalar theories, *Phys. Rev. D* **95**, 125009 (2017).
- [25] Z. Bern, S. Davies, P. Di Vecchia, and J. Nohle, Low-energy behavior of gluons and gravitons from gauge invariance, *Phys. Rev. D* **90**, 084035 (2014).
- [26] V. Lysov, S. Pasterski, and A. Strominger, Low’s Subleading Soft Theorem as a Symmetry of QED, *Phys. Rev. Lett.* **113**, 111601 (2014).
- [27] D. Bonocore and A. Kulesza, Soft photon bremsstrahlung at next-to-leading power, arXiv:2112.08329.
- [28] C. Ewerz, M. Maniatis, and O. Nachtmann, A model for soft high-energy scattering: Tensor pomeron and vector odderon, *Ann. Phys. (Amsterdam)* **342**, 31 (2014).
- [29] V. A. Khoze, J. W. Lamsä, R. Orava, and M. G. Ryskin, Forward physics at the LHC: detecting elastic pp scattering by radiative photons, *J. Instrum.* **6**, P01005 (2011).
- [30] P. Lebedowicz and A. Szczurek, Exclusive diffractive photon bremsstrahlung at the LHC, *Phys. Rev. D* **87**, 114013 (2013).
- [31] V. A. Khoze, A. D. Martin, and M. G. Ryskin, Can invisible objects be ‘seen’ via forward proton detectors at the LHC?, *J. Phys. G* **44**, 055002 (2017).
- [32] A. Cisek, P. Lebedowicz, W. Schäfer, and A. Szczurek, Exclusive production of ω meson in proton-proton collisions at high energies, *Phys. Rev. D* **83**, 114004 (2011).
- [33] P. Lebedowicz and A. Szczurek, Exclusive $pp \rightarrow pp\pi^0$ reaction at high energies, *Phys. Rev. D* **87**, 074037 (2013).
- [34] J. Chwastowski, L. Fulek, R. Kycia, R. Sikora, J. Turnau, A. Cyz, and B. Pawlik, Feasibility studies of exclusive diffractive bremsstrahlung measurement at RHIC energies, *Acta Phys. Pol. B* **46**, 1979 (2015).
- [35] J. J. Chwastowski, S. Czekierda, R. Kycia, R. Staszewski, J. Turnau, and M. Trzebiński, Feasibility studies of the diffractive bremsstrahlung measurement at the LHC, *Eur. Phys. J. C* **76**, 354 (2016).
- [36] J. J. Chwastowski, S. Czekierda, R. Staszewski, and M. Trzebiński, Diffractive bremsstrahlung at high- β^* LHC, *Eur. Phys. J. C* **77**, 216 (2017).
- [37] S. Foroughi-Abari and A. Ritz, Dark sector production via proton bremsstrahlung, *Phys. Rev. D* **105**, 095045 (2022).
- [38] J. L. Feng *et al.*, The forward physics facility at the high-luminosity LHC, arXiv:2203.05090.
- [39] J. D. Bjorken and S. D. Drell, *Relativistic Quantum Fields* (McGraw-Hill, New York, 1965).
- [40] C. Ewerz, P. Lebedowicz, O. Nachtmann, and A. Szczurek, Helicity in proton-proton elastic scattering and the spin structure of the pomeron, *Phys. Lett. B* **763**, 382 (2016).
- [41] L. Adamczyk *et al.* (STAR Collaboration), Single spin asymmetry A_N in polarized proton-proton elastic scattering at $\sqrt{s} = 200$ GeV, *Phys. Lett. B* **719**, 62 (2013).
- [42] D. Britzger, C. Ewerz, S. Glazov, O. Nachtmann, and S. Schmitt, Tensor Pomeron and low- x deep inelastic scattering, *Phys. Rev. D* **100**, 114007 (2019).
- [43] P. D. B. Collins, *An Introduction to Regge Theory and High-Energy Physics* (Cambridge University Press, Cambridge, England, 1977).
- [44] *Regge Theory of Low- p_t Hadronic Interactions*, edited by L. Caneschi (Elsevier Science, Amsterdam, 1989).
- [45] V. N. Gribov, *Strong Interactions of Hadrons at High Energies: Gribov Lectures on Theoretical Physics*, edited by Y. L. Dokshitzer and J. Nyiri (Cambridge University Press, Cambridge, England, 2009); published in Cambridge Monogr. Part. Phys., Nucl. Phys., Cosmol. **27** (2012).
- [46] A. Donnachie, H. G. Dosch, P. V. Landshoff, and O. Nachtmann, Pomeron physics and QCD, Cambridge Monogr. Part. Phys., Nucl. Phys., Cosmol. **19**, 1 (2002).
- [47] A. Donnachie and P. V. Landshoff, Total cross sections, *Phys. Lett. B* **296**, 227 (1992).
- [48] A. Donnachie and P. V. Landshoff, pp and $\bar{p}p$ elastic scattering, *Nucl. Phys.* **B231**, 189 (1984).
- [49] J. Breitweg *et al.* (ZEUS Collaboration), Elastic and proton-dissociative ρ^0 photoproduction at HERA, *Eur. Phys. J. C* **2**, 247 (1998).
- [50] V. Andreev *et al.* (H1 Collaboration), Measurement of exclusive $\pi^+\pi^-$ and ρ^0 meson photoproduction at HERA, *Eur. Phys. J. C* **80**, 1189 (2020).
- [51] L.-J. Zhou, Q. Wu, W.-X. Ma, and Y.-T. Gu, Pomeron-quark coupling from charge conjugation invariance, *Commun. Theor. Phys.* **46**, 287 (2006).
- [52] J. C. Ward, An identity in quantum electrodynamics, *Phys. Rev.* **78**, 182 (1950).
- [53] Y. Takahashi, On the generalized Ward identity, *Nuovo Cimento* **6**, 371 (1957).
- [54] A. Donnachie and P. V. Landshoff, pp and $\bar{p}p$ total cross sections and elastic scattering, *Phys. Lett. B* **727**, 500 (2013); *Phys. Lett. B* **750**, 669 (2015).
- [55] L. Jenkovszky, I. Szanyi, and C.-I. Tan, Shape of proton and the pion cloud, *Eur. Phys. J. A* **54**, 116 (2018).

- [56] L. Jenkovszky, R. Schicker, and I. Szanyi, Elastic and diffractive scatterings in the LHC era, *Int. J. Mod. Phys. E* **27**, 1830005 (2018).
- [57] V. A. Khoze, A. D. Martin, and M. G. Ryskin, Elastic and diffractive scattering at the LHC, *Phys. Lett. B* **784**, 192 (2018).
- [58] E. Martynov and B. Nicolescu, Odderon effects in the differential cross-sections at Tevatron and LHC energies, *Eur. Phys. J. C* **79**, 461 (2019).
- [59] M. Broilo, D. A. Fagundes, E. G. S. Luna, and M. Peláez, Soft Pomeron in light of the LHC correlated data, *Phys. Rev. D* **103**, 014019 (2021).
- [60] N. Bence, A. Lengyel, Z. Tarics, E. Martynov, and G. Tersimonov, Froissaron and maximal odderon with spin-flip in pp and $\bar{p}p$ high energy elastic scattering, *Eur. Phys. J. A* **57**, 265 (2021).
- [61] A. A. Godizov, High-energy elastic diffractive scattering of nucleons in the framework of the two-Reggeon eikonal approximation (from U-70 to LHC), *Eur. Phys. J. C* **82**, 56 (2022).
- [62] G. Antchev *et al.* (TOTEM Collaboration), Measurement of elastic pp scattering at $\sqrt{s} = 8$ TeV in the Coulomb–nuclear interference region: Determination of the ρ -parameter and the total cross-section, *Eur. Phys. J. C* **76**, 661 (2016).
- [63] G. Antchev *et al.* (TOTEM Collaboration), First measurement of elastic, inelastic and total cross-section at $\sqrt{s} = 13$ TeV by TOTEM and overview of cross-section data at LHC energies, *Eur. Phys. J. C* **79**, 103 (2019).
- [64] G. Antchev *et al.* (TOTEM Collaboration), First determination of the ρ parameter at $\sqrt{s} = 13$ TeV: Probing the existence of a colourless C-odd three-gluon compound state, *Eur. Phys. J. C* **79**, 785 (2019).
- [65] P. Zyla *et al.* (Particle Data Group), Review of particle physics, *Prog. Theor. Exp. Phys.* **2020**, 083C01 (2020).
- [66] Data files and plots of cross-sections and related quantities, <https://pdg.lbl.gov/2022/hadronic-xsections/hadron.html>.
- [67] G. Antchev *et al.* (TOTEM Collaboration), Elastic differential cross-section measurement at $\sqrt{s} = 13$ TeV by TOTEM, *Eur. Phys. J. C* **79**, 861 (2019).
- [68] E. Martynov and B. Nicolescu, Did TOTEM experiment discover the Odderon?, *Phys. Lett. B* **778**, 414 (2018).
- [69] E. Martynov and B. Nicolescu, Odderon: Models vs experimental data—a short review of recent papers, [arXiv:1811.07635](https://arxiv.org/abs/1811.07635).
- [70] L. Łukaszuk and B. Nicolescu, A possible interpretation of pp rising total cross-sections, *Lett. Nuovo Cimento* **8**, 405 (1973).
- [71] C. Ewerz, The odderon in quantum chromodynamics, [arXiv:hep-ph/0306137](https://arxiv.org/abs/hep-ph/0306137).
- [72] G. Pancheri, S. Pacetti, and Y. Srivastava, Analysis and implications of precision near-forward TOTEM data, *Phys. Rev. D* **99**, 034014 (2019).
- [73] V. V. Ezhela, V. A. Petrov, N. P. Tkachenko, and A. A. Logunov, On the ρ and σ_{tot} measurement by the TOTEM Collaboration: In the wake of recent discoveries, [arXiv:2003.03817](https://arxiv.org/abs/2003.03817).
- [74] A. Donnachie and P. V. Landshoff, Small t elastic scattering and the ρ parameter, *Phys. Lett. B* **798**, 135008 (2019).
- [75] A. Donnachie and P. V. Landshoff, Lack of evidence for an odderon at small t , *Phys. Lett. B* **831**, 137199 (2022).
- [76] A. Breakstone *et al.*, Measurement of $\bar{p}p$ and pp Elastic Scattering in the Dip Region at $\sqrt{s} = 53$ GeV, *Phys. Rev. Lett.* **54**, 2180 (1985).
- [77] V. M. Abazov *et al.* (TOTEM and D0 Collaborations), Odderon Exchange from Elastic Scattering Differences between pp and $p\bar{p}$ Data at 1.96 TeV and from pp Forward Scattering Measurements, *Phys. Rev. Lett.* **127**, 062003 (2021).
- [78] L. Jenkovszky, O. Kuprash, R. Orava, and A. Saliı̄, Low missing mass, single- and double diffraction dissociation at the LHC, *Phys. At. Nucl.* **77**, 1463 (2014); *Odessa Astron. Pub.* **25**, 102 (2012).
- [79] H. de Kerret, E. Nagy, M. Regler, W. Schmidt-Parzefall, K. R. Schubert *et al.*, Experimental results on diffractive one-pion production at the CERN ISR, *Phys. Lett.* **63B**, 477 (1976).
- [80] A. Bolz, C. Ewerz, M. Maniatis, O. Nachtmann, M. Sauter, and A. Schöning, Photoproduction of $\pi^+\pi^-$ pairs in a model with tensor-pomeron and vector-odderon exchange, *J. High Energy Phys.* **01** (2015) 151.
- [81] P. Lebiedowicz, O. Nachtmann, and A. Szczurek, Searching for the odderon in $pp \rightarrow ppK^+K^-$ and $pp \rightarrow pp\mu^+\mu^-$ reactions in the $\phi(1020)$ resonance region at the LHC, *Phys. Rev. D* **101**, 094012 (2020).
- [82] P. Lebiedowicz, O. Nachtmann, and A. Szczurek, Central exclusive diffractive production of $K^+K^-K^+K^-$ via the intermediate $\phi\phi$ state in proton-proton collisions, *Phys. Rev. D* **99**, 094034 (2019).
- [83] J.-R. Cudell, K. Kang, and S. K. Kim, Bounds on the soft pomeron intercept, *Phys. Lett. B* **395**, 311 (1997).
- [84] E. G. S. Luna and M. J. Menon, Extrema bounds for the soft Pomeron intercept, *Phys. Lett. B* **565**, 123 (2003).
- [85] E. G. S. Luna, M. J. Menon, and J. Montanha, An analysis on extrema and constrained bounds for the soft pomeron intercept, *Nucl. Phys.* **A745**, 104 (2004).